nature reviews physics

https://doi.org/10.1038/s42254-023-00643-7

Roadmap

Check for updates

Progress and prospects in nonlinear extreme-ultraviolet and X-ray optics and spectroscopy

Majed Chergui[1,2] ✉, Martin Beye[3,4], Shaul Mukamel[5], Cristian Svetina[6,7] & Claudio Masciovecchio[2]

Abstract

Free-electron lasers and high-harmonic-generation table-top systems are new sources of extreme-ultraviolet to hard X-ray photons, providing ultrashort pulses that are intense, coherent and tunable. They are enabling a broad range of nonlinear optical and spectroscopic methods at short wavelengths, similar to those developed in the terahertz to ultraviolet regimes over the past 60 years. The extreme-ultraviolet to X-ray wavelengths access core transitions that can provide element and orbital selectivity, structural resolution down to the sub-nanometre scale and, for some methods, high momentum transfers across typical Brillouin zones; the possibilities for polarization control and sub-femtosecond time resolution are opening up new frontiers in research. In this Roadmap, we review the emergence of this field over the past 10 years or so, covering methods such as sum or difference frequency generation and second-harmonic generation, two-photon absorption, stimulated emission or Raman spectroscopy and transient grating spectroscopy. We then discuss the unique opportunities provided by these techniques for probing elementary dynamics in a wide variety of systems.

Sections

[1]Lausanne Centre for Ultrafast Science, Institute of Chemical Sciences and Engineering, Ecole Polytechnique Fédérale de Lausanne, Lausanne, Switzerland. [2]Elettra Sincrotrone Trieste S.C.p.A., Trieste, Italy. [3]Deutsches Elektronen-Synchrotron DESY, Hamburg, Germany. [4]Department of Physics, Stockholm University, Stockholm, Sweden. [5]Department of Chemistry and Department of Physics and Astronomy, University of California, Irvine, CA, USA. [6]Madrid Institute for Advanced Studies, IMDEA Nanociencia, Ciudad Universitaria de Cantoblanco, Madrid, Spain. [7]European XFEL, Holzkoppel 4, Schenefeld, Germany. ✉e-mail: majed.chergui@epfl.ch

Key points

- X-ray free-electron lasers and high-harmonic-generation sources of extreme-ultraviolet (EUV) to hard X-ray photons deliver intense ultrashort pulses and enable the extension of nonlinear methods to much shorter wavelengths.
- EUV to X-ray wavelengths access core transitions that can provide element and orbital selectivity. These wavelengths also achieve sub-nanometre structural resolution and high momentum transfer, with femtosecond and attosecond time resolution.
- Nonlinear EUV/X-ray methods that have emerged include sum or difference frequency generation, parametric down-conversion, second-harmonic generation, two-photon absorption, stimulated emission or Raman spectroscopy and transient grating spectroscopy.
- Nonlinear EUV/X-ray science is developing hand-in-hand with instrumentation, to improve pulse features and enhance accessibility with the use of table-top systems or compact accelerators.
- These techniques offer unique opportunities for probing dynamical events in a wide variety of systems, including surface and interface processes, chirality, nanoscale transport and multidimensional core-level spectroscopy.

Introduction

The invention of the laser in the early 1960s started a revolution in science and technology. One of the most salient developments that ensued was the birth of nonlinear optics, enabled by high-intensity and coherent laser beams. The field began in 1961 with the observation of two-photon absorption (TPA) by Kaiser and Garrett[1] and second-harmonic generation (SHG) by Franken et al.[2] and was recognized in 1981 with the award of the Nobel Prize in Physics to Bloembergen[3]. Nonlinear optics has played a key role in the expansion of laser technology and the birth of photonics and optoelectronics; more broadly, nonlinear methods in the optical domain (ultraviolet, visible, infrared and terahertz frequencies) have led to major advances in experimental and theoretical physics, materials science, chemistry and biology.

Indeed, a wide range of methods have been developed, such as multiphoton absorption that enables excitation of dipole-forbidden transitions and hence widens the spectroscopic analysis of systems. SHG, sum frequency generation (SFG) and difference frequency generation (DFG) processes that arise from the second-order susceptibility of a material ($\chi^{(2)}$; Fig. 1a) — are routinely used in laser laboratories, in particular on non-centrosymmetric samples such as surfaces, interfaces and chiral systems, to provide valuable static and dynamic structural information. In systems that lack inversion symmetry, second-order processes do not occur and the third-order susceptibility ($\chi^{(3)}$) is then the lowest-order nonlinearity. A notable example of a third-order process is third-harmonic generation[4] as a laser beam interacts with a crystal, leading to a tripling of the incoming beam frequency (Fig. 1b). Such four-wave mixing (FWM) techniques enable (through, for example, transient grating spectroscopy) the probing of transport phenomena (such as heat, charge and magnetism) in materials and solutions.

Nonlinear methods have been key to the generation of multicolour pulses for use in fundamental studies. They are also the basis for new imaging techniques — for example, those based on coherent anti-Stokes Raman scattering (CARS) or stimulated emission depletion microscopy — that are finding widespread applications, especially in medicine. They underpin new developments in many fields ranging from metrology to laser machining and from optical communication to optical computers[5]. Pulsed lasers have pushed nonlinear methods to the next level, enabling ever higher peak powers owing to the increased energy per pulse as well as shorter pulse durations. This was recognized by the 2018 Nobel Prize in Physics. Nonlinear methods have therefore become crucial in time-resolved studies, achieving picosecond time resolution by the early 1970s (refs. 6,7) and femtosecond resolution later in the 1970s (ref. 8) — bringing about another revolution as it became possible to access the timescale of nuclear motion within molecules, materials and proteins, a development recognized in 1999 with the award of the Nobel Prize in Chemistry to Zewail[9].

The full breadth of nonlinear laser methods used in both fundamental research and applications is beyond the scope of this Roadmap. Our purpose is rather to examine recent developments that extend nonlinear methods to shorter wavelengths, in the extreme-ultraviolet (EUV) to hard X-ray range. As well as providing element selectivity both in the probing and in the excitation, the short wavelengths offer a structural sensitivity and a change of regime in the definition of symmetry, as the excitations are now localized on atoms rather than on extended orbitals in molecules or bands in a solid.

The advent of EUV, soft and hard X-ray free-electron lasers (FELs and XFELs) over the past 10–15 years[10–14] and the development of table-top EUV light sources based on high-order harmonic generation (HHG)[15–21] are heralding a new revolution in science. The several orders of magnitude increase in photon flux per pulse (for XFELs, typically a factor of 10^6) compared with conventional pulsed X-ray sources such as synchrotrons, along with the pulse duration of femtoseconds to attoseconds commonly achieved by high-harmonic generation (HHG) sources (and nowadays also at XFELs), make these sources game changers for time-resolved X-ray spectroscopic and scattering methods[22–25].

A number of reviews have covered some of these developments for HHG sources and XFELs[25–27]. In this Roadmap, we survey the capabilities of these light sources and the nonlinear methods they enable. We focus on experiments — at photon energies > 50 eV (wavelengths <25 nm) and the current XFEL upper limit of 20 keV — that have been carried out so far on atomic and molecular systems and on solid materials. We then elaborate on new perspectives, guided by technological and theoretical developments. As most of the EUV/X-ray results have been obtained at XFELs, owing to their high photon fluxes, this Roadmap mostly reports work carried out at such facilities. However, important results have also emerged for table-top HHG sources that are milestones in their own right but are also promising for the transfer of EUV/X-ray nonlinear methods from large-scale facilities into university or industrial laboratories.

Instrumentation and methods

Detailed descriptions of the various HHG and XFEL sources of ultrashort EUV/X-ray pulses are available[28–33]. Here, we briefly cover the general characteristics of these sources that are relevant for EUV/X-ray nonlinear methods.

X-ray free-electron lasers

XFEL facilities consist of a linear electron accelerator and a series of undulators (periodic magnetic devices). Electron bunches are accelerated to relativistic speeds and then enter an undulator where they

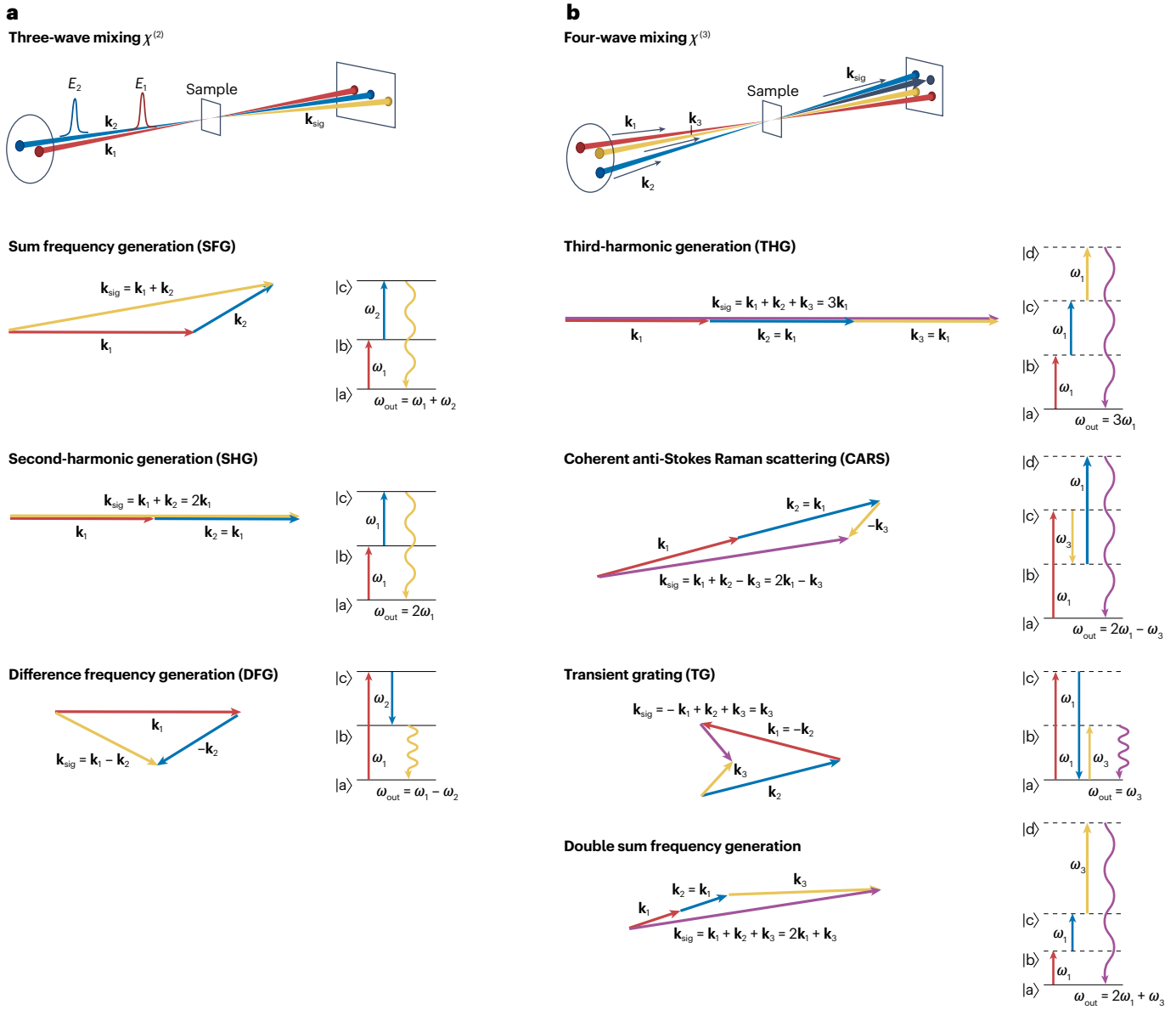

Fig. 1 | Schemes for various examples of nonlinear optical methods. **a**, Three-wave mixing is a second-order process, arising from the second-order susceptibility $\chi^{(2)}$: two incident photons of energies E_1 and E_2 and wave vectors $\mathbf{k}_1$ and $\mathbf{k}_2$ mix to create a third photon, $\mathbf{k}_{sig}$. Examples — represented here as the sum of wave vectors and as transitions between states |a>, |b> and so on — include SFG, in which the frequency of the third photon (ω_{out}) is the sum of the incident frequencies (ω_1 and ω_2); DFG; and SHG, in which $\mathbf{k}_1 = \mathbf{k}_2$ and $\omega_{out} = 2\omega_1$. **b**, Four-wave mixing originates from the third-order susceptibility $\chi^{(3)}$. THG occurs when $\mathbf{k}_1 = \mathbf{k}_2 = \mathbf{k}_3$; for TG, the wave vectors and frequencies of two photons match and ω_{out} matches the (different) frequency of the third photon; the combination for CARS scattering results in $\omega_{out} = 2\omega_1 - \omega_2$; and double sum frequency generation arises when $\mathbf{k}_1 = \mathbf{k}_2$ and $\omega_{out} = 2\omega_1 + \omega_3$. Image courtesy of Andrei Tokmakoff.

undergo a periodically alternating, transverse acceleration that releases photons through the synchrotron process[32,33]. In FELs, the emitted electromagnetic field becomes sufficiently strong that its interaction with the transverse electron current causes some electrons to gain and others to lose energy to the radiation field via the ponderomotive force. This energy modulation evolves into electron density modulations with a period of one wavelength, such that the electron density within a bunch becomes distributed periodically in microbunches. The electrons emit radiation in phase, and the emitted photons add up coherently. The FEL radiation intensity increases, causing additional microbunching; the electrons continue to radiate in phase until they are completely microbunched and saturation is reached, at which point the radiation power is orders of magnitude higher than that of incoherent undulator radiation from a synchrotron. This is known as self-amplified spontaneous emission (SASE)[34]. SASE pulses are characterized by a time-and-energy structure that is the envelope of a series of subpulses with random intensity, time duration, spectral bandwidth and phase. XFEL SASE pulses have durations of tens of femtoseconds and reach

sub-ångstrom wavelengths but have limited temporal coherence, as the initial amplification arises from the electron-beam shot noise.

The first short-wavelength FEL available to users was FLASH at DESY (Hamburg, Germany), launched in 2005. It provided EUV pulses up to 90.5 eV (13.7 nm) and harmonics reaching the water window (280–530 eV)[10]. The first hard X-ray FEL, the Linac Coherent Light Source (LCLS), was launched in 2009 at SLAC (Stanford, CA, USA)[12], soon followed by the EUV-FEL FERMI at Elettra-Sincrotrone Trieste (Trieste, Italy)[35] and the hard XFEL SACLA at the SPring-8 complex (Hyogo, Japan)[13]. In 2017, three additional hard and soft XFELs went into operation: SwissFEL at the Paul Scherrer Institut-PSI (Villigen, Switzerland)[14,36], European XFEL (Hamburg, Germany)[37,38] and PAL-XFEL at Pohang Accelerator Laboratory (Pohang, South Korea)[39], which all operate in the SASE mode[29].

Amplification of coherent emission relies on high-gain harmonic generation, which is obtained by seeding the electron bunch with an external laser pulse that imposes an energy modulation on the electron beam. When that energy modulation is converted into a density modulation, its spectral content includes higher harmonics of the seed laser[40]. This scheme allows full control of the FEL photon output, through the seed laser. Another notable advantage is the preservation of the temporal coherence of the seed laser in the emitted FEL radiation, which ensures that pulses have longitudinal coherence — this is of paramount importance for nonlinear spectroscopic analyses, which require both phase and wavelength manipulation within a given pulse. FERMI is the first machine to use the external seeding scheme, the harmonic up-shifting enabling it to reach output energies >400 eV in the first harmonic, using a cascade scheme or the principle of echo-enabled harmonic generation[41–43] and pulses of tens of femtoseconds duration. A similar scheme is being implemented at FLASH, making use of the higher number of pulses per second possible from superconducting accelerator of FLASH[44]. The soft X-ray ATHOS beamline of SwissFEL has also implemented the seeding scheme, with the goal of reaching even higher energies using echo-enabled harmonic generation; it will deliver pulses with durations of tens to hundreds of attoseconds.

High-harmonic-generation sources

HHG sources appeared at the end of the 1980s and have since become the main sources of attosecond pulses[44,45]. HHG uses an atomic (or even molecular) gas as the medium, which, under strong field ionization, launches free electrons that are accelerated under the influence of an oscillatory laser electric field. Electron–ion recombination, as electrons re-collide with their parent ion, generates EUV photons[46]. Given that the initial ionization occurs during a short time interval around a maximum of the laser electric field, the duration of the generated EUV pulse is a small fraction of that of the driving optical laser pulse — it lies in the attosecond domain. The EUV radiation is generated in the form of a comb of harmonics of the energy of the driving laser, whose cut-off energy scales with the square of the wavelength. Hence, HHG with longer-wavelength laser drivers provides a route to table-top sources of high-energy coherent X-ray pulses[47–49]. Indeed, much effort is being devoted to pushing the spectral range of the HHG sources to higher and higher energies, reaching the nitrogen and oxygen K-edges and even beyond[50,51], as well as increasing the output pulse energy[52]. Furthermore, the increased repetition rate of HHG sources contributes to higher signal-to-noise ratios[53,54].

Although having lower photon fluxes per pulse than XFELs, the table-top nature of HHG sources and their generally higher repetition rates offer more flexibility than XFELs in the planning and performing of experiments. Furthermore, properties of the emitted HHG radiation (such as central frequency, cut-off energy, pulse duration, polarization and so on) can be tailored directly by adjusting the driving laser. The most notable feature of HHG sources remains, however, the generation of attosecond pulses. In addition, advanced schemes based on the synthesis of fields in the infrared have been proposed for the optimization of the attosecond-pulse generation[55]. This would not only take the temporal resolution down to the fundamental timescale of electron motion but also provide a broad spectral bandwidth for spectroscopy[24,56] and high peak powers, which can drive nonlinear processes despite the generally low energy per pulse. Efforts are also underway to perform HHG in solids[57] and liquids[58,59]; however, these dense media lead to lower cut-off energies than gas-phase media do.

Much of the early work focused on the generation process in gases, liquids and solids and on attosecond science per se[15,17,18,46,57,60–67], but, thereafter, studies have evolved towards applications such as ultrafast X-ray absorption spectroscopy[24,25,49,56,68,69], photoelectron spectroscopy in gases[30,70–72], liquids[68,73–76] and solids[77,78] and nonlinear processes such as transient grating spectroscopy[79–83], multiphoton ionization[84,85], pulse compression by FWM[86] and SHG[87].

Different nonlinear schemes enabled by new sources

Under moderate- to high-intensity laser radiation, the macroscopic polarization of matter can be expanded in powers of the external electric-field amplitude[4,88,89], with coefficients $\chi^{(N)}$ (tensors of rank $N+1$) that are commonly referred to as Nth-order susceptibility and that decrease with increasing N, ensuring that the power series converges to a finite polarization. The second-order susceptibility, $\chi^{(2)}$, is the origin of second-order phenomena such as SFG and DFG, which involve the annihilation of two input photons of different frequencies and the generation of a photon at a third frequency, and also SHG, which is a particular case of SFG when the two incident fields have identical frequency[89] (Fig. 1a). $\chi^{(2)}$ is zero for centrosymmetric materials, making SHG, SFG and DFG particularly suited to the study of interfaces and surfaces either statically or dynamically — indeed, optical-domain SHG is one of the most popular second-order nonlinear techniques, commonly used for such purposes[90–93]. Going into a resonance in SHG, SFG or DFG enhances the efficiency of the process and also provides spectroscopic identification[94]: by tuning one of the incoming fields over a vibrational or electronic transition, and detecting its mixing with a second incoming field, the species involved in the dynamics can be determined.

In contrast to $\chi^{(2)}$, the $\chi^{(3)}$ tensors have non-zero elements for any symmetry and each element consists of 48 terms, representing different sequences of the matter density matrix through the process (although in some cases $\chi^{(3)}$ is determined by only a few dominant contributions, owing to symmetry)[95]. FWM is a nonlinear third-order process in which three coherent electromagnetic fields (frequencies $\omega_{1,2,3}$ and wave vectors $\mathbf{k}_{1,2,3}$) interact with a sample to generate a fourth field (ω_4, $\mathbf{k}_4$) that is coherently coupled to the three input fields[88] (Fig. 1b). Each of the three fields induces the sample polarization vector to oscillate at its frequency ω_i ($i = 1$–3), and the excited sample then radiates with a certain phase shift. The interference of the three fields causes beatings at $\omega_4 = \pm\omega_1 \pm \omega_2 \pm \omega_3$, which drive the polarization vector and can be regarded as the radiation source giving rise to the FWM process. This multiplicity of interactions[88,89] makes FWM suitable for studying different types of excitations. Efficient coupling between the four waves only occurs along a specific direction, defined by $\mathbf{k}_4$. Along this direction, the emission from different portions of the excited volume can interfere constructively, as long as the coherence

length of the FWM process exceeds the characteristic dimensions of the interaction volume[88,96,97]. This collective response of the system to the input fields leads to a remarkable increase in the nonlinear signal compared with its linear counterpart, and it may even become dominant for extended samples. However, it is still unclear whether this behaviour, which is well known in the optical regime, is retained at shorter wavelengths.

FWM is the basis of several coherent nonlinear methods, such as coherent Raman scattering, transient grating spectroscopy, multidimensional spectroscopy and impulsive stimulated Rayleigh, Brillouin and Raman scattering, which involve the generation of dynamic (transient) gratings arising from the periodic modulations of optical properties of the sample by different excitations. Coherent Raman scattering is a multiphoton technique for monitoring Raman-active vibrational modes of molecules. It leads to stimulated Raman scattering and CARS, which were theoretically predicted and experimentally realized in the 1960s (refs. 98,99) and have since been used extensively in fundamental studies and microscopy[100].

In transient grating (TG) spectroscopy, an excitation grating (for example, of charge carriers, chemical species, heat or magnetism) is created when two pulses of identical wavelength but with different wave vectors impinge on the sample (Fig. 1b). The decay of the excitation grating is then monitored using a third pulse, which is detected background-free in a direction determined by the phase-matching condition. The grating period is $\lambda/(2\sin\theta)$, in which λ is the wavelength of the incident beams and 2θ is their crossing angle: using shorter wavelengths means smaller grating periods, from micrometre scale at visible wavelengths to sub-nanometre in the hard X-ray regime (Table 1). The disappearance of the excitation grating is often due to diffusion, which has made TG spectroscopy the method of choice for measuring dynamics and transport properties in solids, liquids or gases, with controllable momentum-transfer and background suppression[101].

TG spectroscopy is a first step in the implementation of multidimensional spectroscopies. These were initially developed for NMR spectroscopy in the 1970s (ref. 102) and have since been extended into the optical domain[103], the infrared[104], the visible[105–107] and the ultraviolet[108–110]. In these spectroscopies, the two initially incident pulses have a broad spectral range (or are tunable over a broad range) and are time-delayed with respect to each other; the time-domain measurements can be Fourier-transformed into frequency-domain spectra, which are functions of multiple time delays. These spectroscopies enable the simultaneous observation of multiple chromophores and/or transitions in a system, and their evolution with time, which may reflect crosstalk between chromophores. Extending these spectroscopies into the region of core-level transitions would enable the monitoring of time-evolving interactions with element selectivity between atoms in a system.

Consideration of the capabilities of short-wavelength nonlinear methods began more than half a century ago — in particular, for X-ray and optical wave mixing[111–117]. The process is akin to optically modulated X-ray diffraction in which X-rays scatter inelastically from optically induced charge oscillations and therefore probe optically polarized charge. The first experimental realization of nonlinear X-ray methods was achieved in the early 1980s, as hard X-ray to EUV parametric down-conversion (PDC) using an X-ray tube as source[118]. Theoretical studies were undertaken systematically from the early 2000s[119–126]. One of the first attempts to demonstrate FWM at EUV energies was carried out using an HHG source[127]. With the advent of XFELs, several developments have made it possible to implement nonlinear EUV/X-ray experiments, as discussed in the next section.

Extending nonlinear science into the short-wavelength regime brings several advantages in terms of accessible core transitions, spatial resolution and momentum transfer (in the case of transient grating spectroscopy) that are summarized in Table 1. Depending on the element, the various spectral regimes access different core transitions, such as the M-edges of 3*d* transition metals for the EUV, the K-edges of light elements (such as carbon, nitrogen and oxygen) or the L-edges of 3*d* transition metals in the soft X-ray range and the K-edges and L-edges of metals in the hard X-ray range. In addition, heterodyne detection[128,129] should be possible, which will enable the amplitude and phase terms of a signal to be disentangled, retrieving the real and imaginary components of the nonlinear susceptibilities in the EUV/X-ray range.

Applications

Two-photon absorption and transient absorption

TPA was one of the first nonlinear techniques to follow from the invention of the laser[1]. Moving into the EUV/X-ray domain, however, involves a considerable decrease of nonlinear susceptibility: for example, going from visible frequencies to keV photons implies at least a 1,000-fold decrease in the TPA cross-section[122]. In addition, it is not even clear whether hard X-ray TPA is dominated by the same mechanisms as in the optical or even soft X-ray domains. But XFELs (with high fluxes) and HHG sources (with attosecond-pulse durations) can deliver the high peak powers needed to compensate for the low nonlinear susceptibility.

Because of its selection rules, TPA accesses partially or fully dipole-forbidden transitions, thus providing information complementary to that obtained using one-photon absorption. Short-wavelength TPA can also act as an instantaneous probe of excited-state dynamics with chemical specificity, as well as providing better sensitivity for K-shell spectroscopy to connect to the *d*-states.

Early TPA studies were carried out in the EUV at FLASH[130], then at the LCLS in the soft X-ray regime[122,131] on rare gas atoms. Nonlinear processes competing on the Auger timescale were observed: two-photon,

Table 1 | Comparison of transient grating spectroscopy in different regimes

Regime	Energy range (eV)	Momentum transfer (nm^{-1})	Spatial scale (nm)	Timescale	Selectivity
Infrared–optical–ultraviolet	<5–10	<0.02	>125	More than a few femtoseconds	Valence shells
EUV	10–150	<0.6	>5	A few femtoseconds to attoseconds	Mostly M shells
Soft X-ray	150–2,500	<25	>0.2	Femtoseconds to attoseconds	L, M shells
Hard X-ray	2,500–20,000	<200	>0.03	Femtoseconds to attoseconds	K, L, M shells

Potentially reachable momentum transfer, spatial and time resolution and selectivity (for 3*d* transition metals) are shown for the infrared–optical–ultraviolet, extreme-ultraviolet and soft and hard X-ray regions. EUV, extreme-ultraviolet.

one-electron direct ionization and two-photon, two-electron sequential ionization involving transient excited states. The TPA cross-section was found to be two to three orders of magnitude larger than theoretically predicted (using non-resonant perturbative scaling[132] or second-order perturbation theory[133]), which was attributed to contributions from near-resonant states[134].

In the hard X-ray regime, TPA was reported at 5.6 keV on germanium at SACLA[135]. The detected signal was the Ge K_α emission, which can be excited by photons above 11.1 keV. It was concluded that TPA competes with single and sequential multiphoton processes as in atoms[122,130,131], and the results were consistent with non-resonant hydrogen-like Z^{-6} scaling (in which Z is the atomic number). This outcome was confirmed in an experiment on zirconium at SACLA that used a nanometre-scale focal spot near 9 keV, half the photon energy of the Zr K-edge[136]. When iron and copper foils were illuminated with intense X-ray pulses near their respective K-edges, emission at nearly twice the incoming photon energy was reported[125], showing a quadratic dependence with the incoming intensity that is typical of TPA. Sample damage occurs, mainly caused by one-photon absorption owing to the high incident fluxes required for TPA. Using lower pulse energies and fluxes than in ref. 136, and a shorter pulse duration and more efficient detection at SACLA, the pulse energy dependence of TPA in metallic copper was reported by detecting the Cu K_α emission[137].

Saturable transient absorption (STA) is a nonlinear pump–probe technique that exhibits a reduction in the relative absorption of the sample (that is, an increase in transmission) with increasing incident light intensity. STA is strongly intertwined with TPA and, depending on the resonances, one or the other processes becomes dominant. This phenomenon has widely been demonstrated in the visible and infrared ranges[138], and saturable absorbers have a key role in the passive mode-locking of femtosecond laser oscillators[139]. Because STA is highly sensitive to the electronic states of the material under study, it is often used as a probe of dynamics and recovery in pump–probe experiments. For example, it has been used to investigate exciton–exciton annihilation[140] or charge carrier dynamics and diffusion[141].

Optical-domain STA involves valence electronic states, whereas in the EUV/X-ray range, core transitions are involved, offering the possibility to investigate the underlying processes with element selectivity. Such studies have been reported at FELs in which the STA of the L-shell transition of aluminium was observed with photon energies of 92 eV (13 nm)[142], followed by observations at the tin N-edge at 24 eV (52 nm)[143] and in the hard X-ray range, at the iron K-edge at 7.1 keV (0.17 nm)[144]. In these studies, STA was attributed to depletion of the ground state by the intense pulses, leading to X-ray-induced transparency. The intensity threshold for the latter depends on the core-transition energy. Transitions from deeper core shells have a shorter core-hole lifetime, thus increasing the intensity necessary to observe STA. In a recent study, graphite films were investigated using soft X-ray FEL pulses of varying intensity[145]: at lower intensities, the nonlinear contribution to the absorption was dominated by STA, owing to ground-state depletion, but for higher intensities ($>10^{14}$ W cm^{-2}), TPA became dominant.

Although the feasibility of TPA and STA in the EUV/X-ray domains is now established, further studies are needed to expand the range of their applications.

Stimulated X-ray emission and Raman processes

X-ray emission and X-ray Raman spectroscopy can provide information about the energy and dispersion of the elementary low-energy excitations (vibronic, charge, magnon and orbital excitations). The low emission yield of these techniques calls for intense XFEL excitation pulses with, just as for TPA, risks of sample damage. This can be circumvented by stimulating the process with a second pulse.

Stimulated emission from a single X-ray fluorescence line in a neon gas was reported shortly after the advent of XFELs[146]. Soon after came the demonstration of stimulated X-ray emission from a solid-state sample at the FLASH XFEL under non-resonant silicon L-edge excitation at an energy of 115 eV (ref. 147). The latter produces regions with high $2p$-core-excitation densities, and the spontaneously emitted radiation from recombination of the $2p$-core holes (photon energy of 85 eV to ~100 eV) seeds the stimulated emission of soft X-ray photons. The emission spectrum is determined by a spontaneous process as in typical resonant inelastic X-ray scattering (RIXS) or X-ray emission spectroscopy and thus the spectrum conserves all the information and specificity of these methods. By carefully choosing the geometry, the weak fluorescence signal was substantially enhanced at the expense of Auger decay, implying minimized electronic damage to the sample. More recently, stimulated EUV emission was reported from solid magnesium oxide at FERMI[148]. For a hard X-ray inner-shell atomic laser with a copper target pumped by FEL pulses[149], the dependence of the output energy versus the pump pulse energy, detected in transmission geometry, exhibited a nonlinear enhancement from a pumping threshold, typical of amplified stimulated emission.

K-shell excitation leads to the K_α, K_β and K_{VtC} (valence-to-core) emission lines. K_α and K_β emission carries information about the electronic and spin structure of the system, and K_{VtC} additionally contains fingerprints of the chemical bonding of the atoms with their neighbours, their oxidation state, covalency and so on[150]. However, K_β lines are typically an order of magnitude weaker than K_α lines, and K_{VtC} lines are two to three orders of magnitude weaker than the K_α lines. Time-domain spontaneous K_α and K_β emissions have already been used to probe molecular dynamics with femtosecond resolution[151–153]; K_{VtC} emission was also observed with picosecond resolution at synchrotrons[154] and with femtosecond resolution at XFELs[155]. By externally stimulating the K_β or K_{VtC} transitions, one could enhance the sensitivity of such experiments. An observation and analysis of the gain curve of amplified K_α emission from solutions of Mn(II) and Mn(VII) complexes showed spectra at amplification levels extending over four orders of magnitude until saturation, and bandwidths below the Mn 1s core-hole lifetime broadening in the onset of the stimulated emission[156]. In a more recent work,[157] seeded amplified K_β emission was also reported from an $NaMnO_4$ solution using two-colour XFEL pulses: the first creates the 1s core-hole population inversion and the second seeds the amplified K_β emission. The latter showed a signal enhancement of $>10^5$ with respect to the conventional K_β emission, within the same solid angle. The upcoming attosecond XFEL pulses[158] promise to beat the core-hole lifetime and drive the system into amplification of specific emission lines.

Femtosecond stimulated Raman spectroscopy is a nonlinear optical method that has been implemented for the study of vibrational dynamics with high spectral and temporal resolution[159,160]. In the X-ray regime, RIXS[150,161–163] is an ideal tool for populating electronic valence states that are inaccessible by direct excitation in the ultraviolet–visible domain. Stimulated RIXS (SRIXS) has therefore the potential of significantly populating such states[164] and when driven by attosecond pulses, it would enable direct probing of valence electron wave packets[121,165,166] or of coupled nuclear–electronic motion on attosecond timescales[167].

SRIXS was first achieved for atoms[168,169] and more recently in diatomic molecules such as carbon monoxide[170] or nitric oxide[171].

The use of attosecond X-ray pulses induced electronic population transfer via SRIXS using the broad spectral bandwidth (5.5 eV full width at half maximum). The impulsive excitation was resonantly enhanced by the oxygen $1s \rightarrow 2\pi^*$ resonance of nitric oxide, and the excited states of the neutral molecules were probed with a time-delayed ultraviolet pulse.

Stimulated resonant elastic X-ray scattering and SRIXS have been reported near the cobalt L_3-edge (770–785 eV) in solid Co–Pd multilayer samples. An enhancement of four to five orders of magnitude of the stimulated over the spontaneous RIXS signal was reported[172]. However, for both signals, contributions from inelastic electron-scattering processes were observed, even for very short pulses, which result in valence-electron redistribution effects that distort the stimulated elastic and inelastic spectra owing to overlapping spectral changes. Therefore, a detailed characterization of these effects is needed to establish SRIXS as a tool for the study of low-lying excitations in solids.

We have already mentioned the two-photon study[125] on Cu and Fe foils, which were excited with photons of energy from just below the relevant single K-shell threshold to well above the sequential double K-shell threshold, and the measurements included higher-energy photons below twice the input energy. The spectrum of emitted high-energy photons showed both dispersive and non-dispersive lines that were attributed to double-core-hole-mediated resonant X-ray Raman scattering, analogous to hyper-Raman scattering, and two-electron–one-photon fluorescence. This can be considered as an anti-Stokes process from a core-excited intermediate state in which the excess energy is taken up by one or more photoelectrons and lines. In all cases, K-shell electrons are excited and subsequently de-excited during the process.

Sum and difference frequency generation

In the X-ray domain, SFG and DFG are akin to optically modulated X-ray diffraction in which X-rays inelastically scatter from optically induced charge oscillations and therefore probe optically polarized charge. This enables the optically induced microscopic field to be determined, as it is closely related to the induced charge[173,174]. Although the idea has been around for a long time[111–117], and further theoretical developments have been made[120,123,124,175,176], the experimental verification of such processes had to wait for the advent of XFELs.

A pioneering experiment demonstrated X-ray/optical SFG in a single crystal of diamond[177]. Optically modulated X-ray diffraction from the (111) plane generated a pulse at the sum frequency of the incident optical (1.55 eV) and X-ray (8 keV) pulses. To increase the efficiency and access the atomic-scale motions, the process is phase-matched using a reciprocal lattice vector. The phase-matching geometry determines the direction of the generated photon, slightly offset from the Bragg diffracted beam, which should allow the induced charge distribution to be reconstructed. The implications of this work are far reaching: it shows that X-ray/optical SFG provides simultaneous access to the induced charges and the associated microscopic fields that arise when light illuminates a material. It also paves the way for X-ray/optical–EUV SFG and DFG processes to study the ultrafast dynamics at surfaces and interfaces by directly probing valence charges on atomic timescales and length scales. The information content of such experiments can be considered in close analogy to spontaneous RIXS experiments, but the achievable signal levels should be substantially enhanced in the nonlinear process through the coherent mixing of the involved fields and the associated phase-matching conditions (Fig. 2). However, generalization of optical/X-ray SFG is challenging because of its low efficiency, which depends linearly on the intensity of the optical laser.

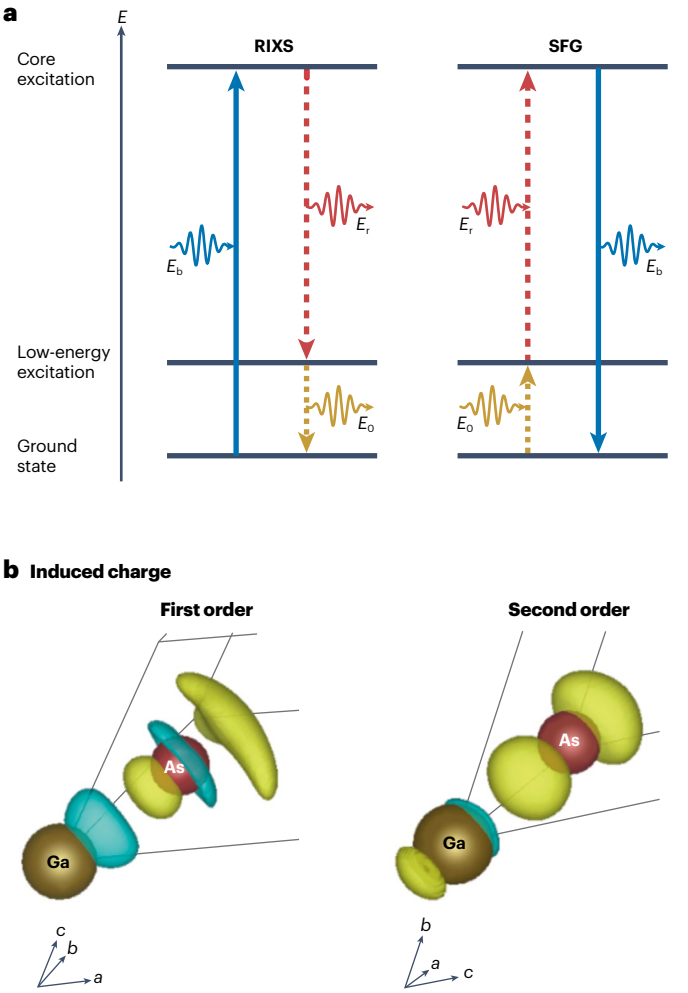

Fig. 2 | Incoherent resonant inelastic X-ray scattering versus coherent sum frequency generation. a, Comparison of the spontaneous and incoherent process of resonant inelastic X-ray scattering (RIXS) and the stimulated coherent process of sum frequency generation (SFG). In a RIXS process, the element-selective core-excitation (of energy E_b) decays spontaneously into a low-energy excitation (E_0). The near isotropically emitted photons must be energy-resolved to determine the energy loss (E_r). In SFG instead, the coherent interaction of the optical and X-ray beams couples the low-energy excitation with the core excitation (E_0 and E_r). The SFG photon (E_b) is emitted into the background-free phase-matching direction and it does not need to be energy-resolved. To map out the low-energy excitation spectrum for a given core excitation, the optical and X-ray photon energies both need to be scanned synchronously. **b**, Calculated[265] first-order and second-order amplitudes of the induced charge density oscillations in GaAs for an optical field polarized along the [111] direction. Yellow indicates the electron density and blue indicates the hole density. Higher-order X-ray/optical sum frequency generation potential to become a novel time-resolved probe for light-induced charge dynamics in solids on the atomic scale. Part **a** is reprinted from ref. 264 under a Creative Commons licence CC BY 4.0; part **b** is reprinted from ref. 265 under a Creative Commons licence CC BY 4.0.

Therefore, it requires optical intensities that are often larger than the radiation damage threshold of most materials, which also need to be optically transparent, therefore limiting the range of systems that can be investigated.

We earlier mentioned PDC, which is similar to X-ray or EUV/optical DFG: in the first such experiment[118], using the 002 reflection of an LiF single crystal, phase-matched PDC of 8 keV (Cu-K_α) photons from a commercial rotating anode into single photons at 7.7 keV was achieved, with idler photons in the EUV at 335 eV. This work was followed by X-ray to EUV PDC studies at synchrotrons[178–180] that demonstrated, in particular, that one can visualize the local optical response to EUV radiation with atomic resolution[180]. Extending X-ray PDC to the optical domain — X-ray PDC from 11 keV to 3–4 eV photons at a synchrotron has been reported[181] — could provide a powerful probe of charge oscillations, for example, in phenomena associated with energies near the Fermi level of metals or near the bandgap of semiconductors.

Overall, one of the key advantages of optical/EUV or optical/X-ray SFG and DFG is that the optical pulse can be tuned to vibrational or valence resonances, whereas the EUV/X-ray pulse can be tuned to specific core transitions. This tunability provides enhanced flexibility in terms of resonance conditions corresponding to vibrational or electronic transitions and core transitions for systems lacking inversion symmetry. Further enhancement of signals can be achieved using, for example, plasmonics in the case of electronic resonances.

Second-harmonic generation

Extending SHG into the EUV/X-ray domain offers the additional advantage of element selectivity. Furthermore, the theory of X-ray nonlinearities in solids[111,112,115] assumes that, because all pertinent photon energies are much higher than the binding energies of the electrons in light elements, the electrons can be treated as free particles, and the dominant nonlinearity is plasma-like. EUV/X-ray SHG might thus provide a new window into electron densities in the future. This nonlinearity is different from the optical-domain nonlinearities in that it is non-local, second-order and can be observed in centrosymmetric materials, provided that the electron density is non-uniform.

In EUV/X-ray SHG spectroscopy, the incident beam is resonant or half-resonant with a core-to-valence transition, such that the resulting, resonantly enhanced, background-free signal is sensitive to core levels (Fig. 3a). By frequency-resolving the SHG radiation, the symmetry breaking can be correlated to particular spectral features. The first demonstration of short-wavelength SHG was made on a diamond crystal using 7.3-keV photons from the SACLA XFEL with a pump intensity of 10^{16} W cm^{-2} (ref. 182). An SHG efficiency of 5.8×10^{-11} was reported. This work was followed by SHG near the carbon K-edge (~284 eV) in transmission geometry (Fig. 3b) on graphite thin films at FERMI[183]: the experimental results and theoretical analysis highlighted the effect of resonant enhancement above the C K-edge and showed the interfacial sensitivity of the technique in a centrosymmetric sample with the second-harmonic intensity predominantly arising from the first atomic surface layer.

SHG was demonstrated[184] from a non-centrosymmetric bulk crystal of $GaFeO_3$ using EUV pulses from the SACLA XFEL. The XFEL photon energy was set to half the energy of the Fe 3*p* absorption (M-) edge (~53 eV) and the SHG signals were enhanced by a double-resonance effect met by the O 2*s* → Fe 3*d* (interband) and the Fe 3*p* → O 2*s* (intraband) transitions (Fig. 3c,d). This enhancement offers exciting leverage in the study of transition metal oxides, in which it is possible to satisfy the double resonance between the O L_1-edges and metal M-edges and thus enhance the signal. Note that, in contrast to Fig. 3b, this work was carried out in reflection geometry, for which the wave vectors along the sample surface are required to match (a condition that is automatically satisfied) and the momentum transfer of the sample in the normal direction does not give a critical condition in the regime in which the wavelength is longer than the attenuation length. This points to possible application of the method to diverse samples and experimental conditions. The same reflection geometry was implemented to investigate the broken inversion symmetry in the polar metal phase of $LiOsO_3$, revealing an enhanced feature above the Li K-edge that reflects the degree of Li atom displacement[185].

Probing buried interfaces using optical methods can be challenging and does not provide element-specific information. Recently, EUV-SHG was used around 190 eV at FERMI to probe the buried interface of a boron film with a support layer of parylene N, a prototypical inorganic–organic interface. The experiment revealed distinct spectral features that are not observed in X-ray absorption spectra, demonstrating its extraordinary interfacial sensitivity. With the help of electronic structure calculations, the boron–organic separation distance was derived, but most important, sub-ångstrom changes were shown to translate into spectral shifts of the order of hundreds of millielectron volts that are easily detected by EUV-SHG[186].

HHG sources have also been used to carry out ultrafast SHG experiments in the EUV, including one performed above the Ti M-edge (32.6 eV) of solid titanium using high-power HHG sources[87]. Comparison of the observations with calculations using density functional perturbation theory and real-time time-dependent density functional theory suggested resonant contributions from Ti 3*p* to Ti 3*d* transitions to the SHG signal at the Ti surface.

In summary, although EUV-SHG is still interface-sensitive, hard X-ray SHG seems to respond to the bulk in the case of non-centrosymmetric crystals. A systematic investigation of such phenomena would widen the range of applications of EUV/X-ray SHG and even of SFG and DFG methods.

Four-wave mixing

Extending FWM techniques into the EUV/X-ray domain brings fresh insight into the electronic structure and dynamics of the systems under study.

Before the XFEL era, studies using EUV-HHG pulses had demonstrated the coupling of fields either all-EUV as in ref. 127 or optical and EUV[79,80,82,83,187]. In the latter cases, the transient grating was generated by optical pulses and the EUV-HHG radiation by a third optical pulse within the excited fringes. Exploiting the grating to disperse the various harmonics offered an elegant way of monitoring the rotational wave packets of molecular systems[82], as the HHG signal is sensitive to the alignment of the molecule with respect to the laser polarization. An insightful use of FWM was demonstrated by combining an attosecond EUV-HHG pulse and two separately timed, few-cycle, near-infrared pulses[188], to characterize the dynamics of the Na^+ $L_{2,3}$-edge core excitons in NaCl. An inhomogeneous distribution of core excitons underlying the Na^+ Γ-point spectrum was deconvolved by resonance-enhanced FWM. In addition, dark excitonic states that are coupled to the EUV-allowed levels by the near-infrared pulses were characterized spectrally and temporally. The coherence lifetime of the core-exciton states was <10 fs.

An experiment at FLASH[189] extended a similar mixing of two optical photons with an EUV photon on an LiF sample. Instead of analysing the spatial dependence of the emitted EUV at the same wavelength as the incoming beam, a colinear scheme of optical laser and EUV FEL was used, but the emitted photons were observed at energies offset from the incoming EUV by two optical laser photons, in both an SFG scheme and a DFG scheme. Strong enhancements of the signal at the

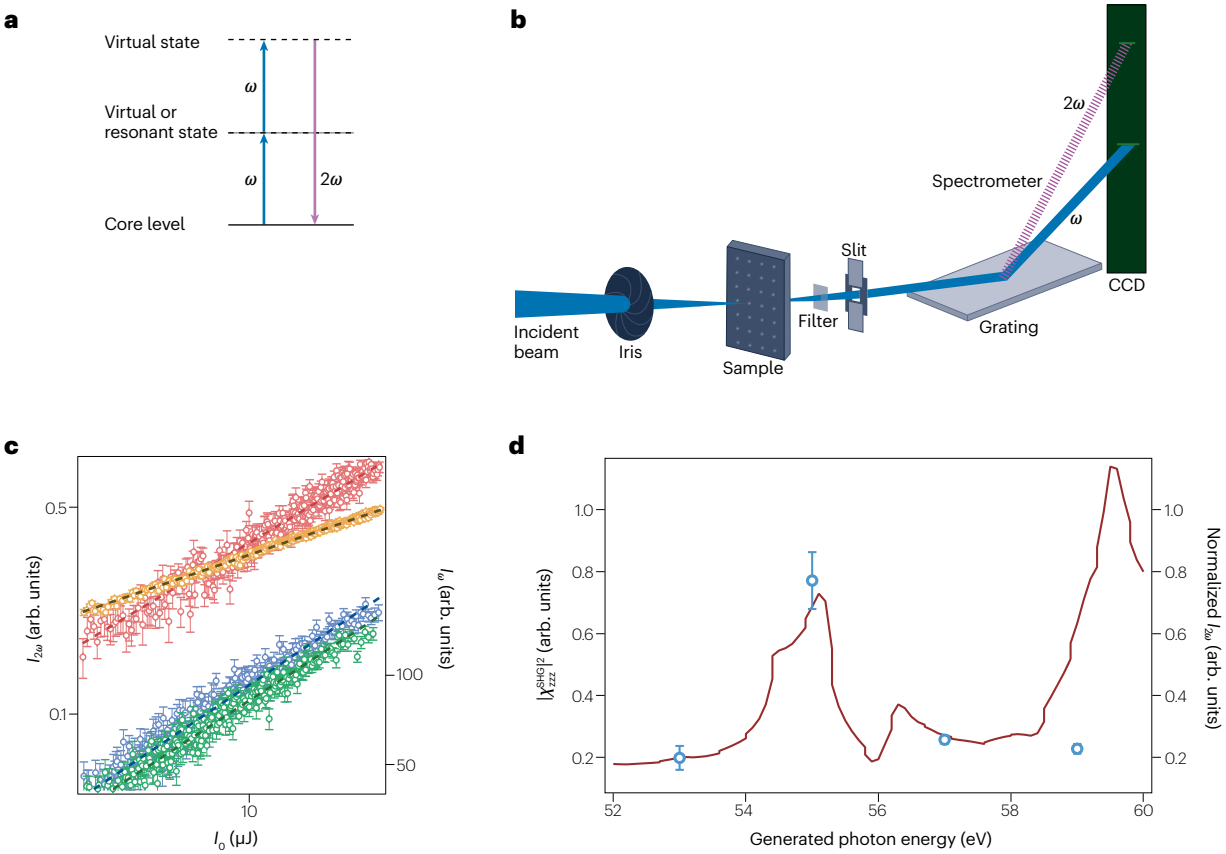

Fig. 3 | Extreme-ultraviolet and X-ray second-harmonic generation. a, Energy-level scheme for EUV/X-ray second-harmonic generation (SHG): two input photons of frequency ω generate a third photon of frequency 2ω. **b**, In the transmission configuration for SHG experiments, the incident beam is focused onto the sample, and the transmitted beam and the collinear second-harmonic signal (at double the fundamental photon frequency, 2ω) are dispersed by a grating that spatially separates the second-harmonic signal from the fundamental, which are imaged on a charge-coupled-device (CCD) camera. A reflection geometry, rather than the transmission through the sample shown here, has also been used[184]. **c**, In the case of EUV-SHG on a $GaFeO_3$ crystal, the SHG signal $I_{2\omega}$ has a quadratic dependence on the incident power I_0, measured using the photoionization of Ar gas in a shot-by-shot manner (note the logarithmic scale). $I_{2\omega}$ is shown for photon energy of $2\hbar\omega = 55$ eV (red circles), 57 eV (blue circles) and 59 eV (green circles); I_ω (orange circles) is the signal of the reflected incident beam at the incident energy of $\hbar\omega = 27.5$ eV. Dashed lines indicate a power-law fit. The error bars reflect the uncertainty in the measured SHG signal. **d**, The SHG signal (green data points) is enhanced around 55 eV by the double resonant effect of the transition between O 2*s* → Fe 3*d* and between the Fe 3*p* → O 2*s* state. (In the SHG spectrum near the Fe 3*p*-edge for $GaFeO_3$, there are contributions from the inner-shell double resonance at the 3*p*-edge position and interband transitions that give a tail structure in the post-edge region.) The red line represents calculated values of the square of the second-order susceptibility tensor $\left|\chi^{SHG}_{zzz}\right|^2$. Parts **a** and **b** reprinted with permission from ref. 183, APS; parts **c** and **d** reprinted with permission from ref. 184, APS.

Li 1*s* resonance were observed when either the incoming EUV pulse or the emitted EUV photons hit the resonance. The signal strength increased where the localized excitonic EUV resonances overlapped with an optically induced local resonance, but were below the detection threshold at delocalized band structure features. This result opens a new window into probing the localization degree of excitations in matter using nonlinear spectroscopy and provides an experimental step towards realizing more complex experiments (Fig. 2).

X-ray diffraction has long been used to probe optically induced transient gratings in synchrotron-based experiments. The X-ray pulse can probe the grating at a spatial resolution limited by the grating period. The amplitude of transient surface deformations was determined with sub-ångstrom resolution, and control of the amplitude and the phase of a thermally deformed surface was achieved[190,191]. This approach has also been used to study photoinduced strain (structural grating) with an amplitude proportional to the optical flux, as well as magneto-structural phase transformations[192].

Of the various short-wavelength FWM schemes (Fig. 1), TG spectroscopy has emerged as one of the most popular as it offers element specificity, smaller nanometre-scale grating periods and large momentum transfers (Table 1) and also access to new kinematic regions (Fig. 4). Indeed, in such experiments, the temporal information about the low-order nonlinear light–matter interaction is mapped into the spatial domain where it can be observed against a zero background[4]. This enables measurements in which only a small fraction of the molecules is excited, as is the case for typical diffracted signals (for more details, see Figs. 5 and 6). To fully benefit from the capabilities of EUV/X-ray TG spectroscopy, the probe pulse must also be in the EUV or X-ray range, which means controlling two such pulses in energy and time — a task that remains challenging.

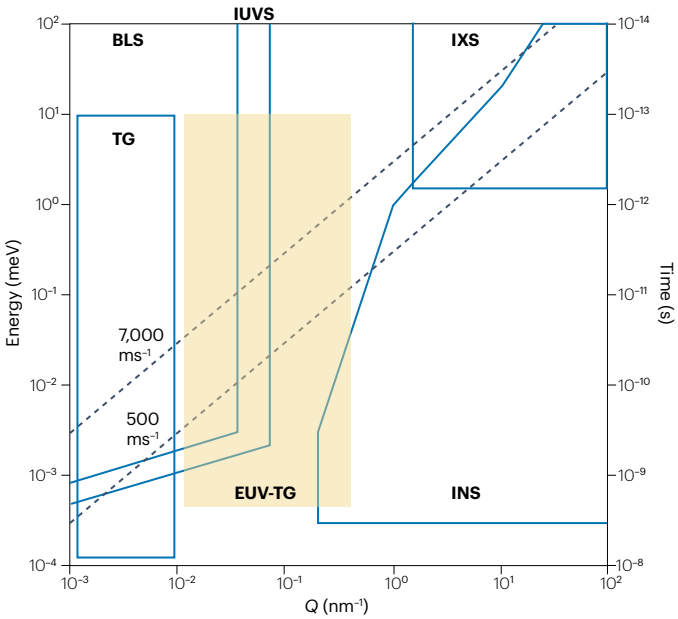

Fig. 4 | Kinematic regions that are accessible using existing techniques. In energy, timescale and momentum transfer (Q), accessible regions are indicated for transient grating (TG), Brillouin light scattering (BLS), inelastic ultraviolet scattering (IUVS), inelastic X-ray scattering (IXS) and inelastic neutron scattering (INS). Highlighted is the region that becomes accessible using extreme-ultraviolet transient grating (EUV-TG). Dotted lines indicate energies of collective excitations with characteristic speeds of sound of 500 ms^{-1} and 7,000 ms^{-1}, which are commonly associated with, respectively, low-density (such as gases) and high-density (such as glasses) disordered systems. Adapted with permission from ref. 309, Elsevier.

However, a first major step has been taken[193], using two ultrashort (60–80 fs) EUV (27.6 nm) pulses from the FERMI FEL to generate a TG on a SiO_2 glass and then probe it with a ~100-fs optical beam at 392.8 nm. The results (Fig. 6b) clearly show the electronic response at time $t = 0$, followed by an appreciable signal up to $\Delta t = 130$ ps. For $\Delta t > 10$ ps, the signal was ascribed to thermal relaxation and longitudinal acoustic modes, whereas at shorter times (<1.6 ps), coherent oscillations owing to optical (Raman) phonon modes were observed, demonstrating that EUV TGs can drive coherent excitations in the sample, an observation that was confirmed on other systems.

Probing an EUV-generated TG with an optical pulse severely limits the spatial resolution, as already mentioned. Therefore, in a subsequent experiment[194,195], the FERMI team demonstrated all-EUV TG (Fig. 5a) on silicon or silicon nitride. The third EUV probe pulse was time-delayed with respect to the first two but was of identical energy. The time between the pump and the probe pulses was tuned using the split-and-delay scheme shown in Fig. 5a. The signal exhibits coherent phonon oscillations on top of a slowly decaying background (Fig. 6a). The latter, along with the damping of the oscillations, are related to the thermal equilibration time. Most remarkable is the absence of the electronic response peak at $t = 0$, which occurs in the all-optical or optically probed EUV TGs[193] (Fig. 6b). This is because refractive index changes at optical wavelengths are highly sensitive to electronic excitations of the conduction or valence band, whereas at EUV wavelengths, they are mostly sensitive to changes in the total electronic density, making the all-EUV transient grating signal sensitive to the structural response. This offers a way of distinguishing electronic and nuclear responses in materials.

The demonstration of EUV TGs[193,195] led to a flurry of studies on the generation of coherent acoustic and optical phonons[196,197]; the element specificity of the EUV-generated resonant TG[198]; the probing of thermoelastic properties of materials[199] and the generation, control and probing of magnetic patterns[200,201]. The latter three studies used an all-EUV TG configuration. The work on magnetization TGs, with periods of a few tens of nanometres in a CoGd alloy[200], was carried out using two pump energies: one resonant with the M-edge of Co and the other (non-resonant) at half the energy of the first. In both cases, the probing was resonant with the M-edge of Co. It was found that the patterns of a sample magnetized to saturation (by an external static magnetic field) appear on a sub-picosecond timescale (similar to the electron–phonon relaxation in a metal) as the sample is thermally demagnetized by the EUV transient grating; they decay on timescales of tens of picoseconds, suggesting that thermal transport is the leading mechanism that erases the magnetization grating. The transient grating period dependence was investigated (Fig. 6c), indicating a transport process. Indeed, on the timescales of the decay, the lattice, electronic and spin systems are in thermal equilibrium, and as the temperature grating is erased by thermal diffusion, the magnetization grating also decays. This result is also a clear manifestation of the effect of the grating periodicity on the transport kinetics.

Going to the shorter wavelength regime of hard X-rays opens up an even smaller range of nanoscale grating periods (Table 1), for which the nature of transport and, in particular, the crossover from ballistic to diffusive transport are largely unexplored. The challenge in this spectral domain is the lack of reflective optics — but this has been circumvented[202,203] using diffractive optics, namely, the Talbot effect (Fig. 5b), first to demonstrate the formation of permanent gratings on solid samples using 3-keV photons from the SwissFEL[203] and then to create a TG in bismuth germanate at 7 keV, which was probed by an optical pulse at 400 nm (ref. 202). This experiment demonstrated hard X-ray TG spectroscopy, with the signal (Fig. 6d) exhibiting the same optical phonons as in the non-resonant EUV-transient grating experiment discussed earlier[196]. In the latter case, they were attributed to a displacive excitation and in optical experiments to impulsive stimulated Raman scattering[204], but the mechanism in the case of hard X-rays is yet to be determined.

More recently, hard X-ray TG generation was achieved[205] by crossing two X-ray 30-fs beams generated by an X-ray split-delay line (Fig. 5a) at LCLS[206]; the TG was then probed by an optical pulse. This result opens the possibility of delaying one of the two pump pulses and performing frequency-resolved optical-gating (FROG) detection of X-ray TG measurements — an important development towards multidimensional core-level spectroscopy.

It has been shown that hard X-rays can interact and even manipulate magnetic orders (such as domains), just like EUV radiation but with the advantage of smaller grating periods, down to a few nanometres[207]. For example, manipulation of magnetic domains has been achieved through impinging high-intensity permanent gratings at 7 keV in a sample of thulium-substituted yttrium iron garnet with perpendicular magnetic anisotropy. This experiment also indicates that by reducing the X-ray flux, transient excitation of magnetic orders, such as magnons, can be triggered and subsequent dynamics can be probed at the characteristic scales of the collective excitations. Although using permanent gratings, this experiment implies that magnetic TGs could also be generated using hard X-rays with nanoscale periods.

The latest experiments have explored optically probed hard X-ray TG spectroscopy in solutions and all-hard X-ray TG spectroscopy in solids; results are being analysed at present.

Theoretical developments

Emerging nonlinear experimental capabilities, and the advances they entail, require robust theoretical and computational tools to model and support the interpretation of signals, as well as to inspire innovative experiments[208]. These studies operate either in the static regime, developing and utilizing efficient and accurate electronic-structure methods for the calculation of core-hole states[209–212], or in the time-dependent regime through the calculation of molecular dynamics using different numerical methods[213–218]. The computation of time-resolved X-ray signals poses theoretical challenges such as accurate and practical calculations of core-excitation energies[210–212,219–224], which are required to pre-screen possible experiments and make optimal use of beam time.

The idea to probe optically induced charge distributions using optical/X-ray wave-mixing dates back to the 1970s[111–113,117,225]. Subsequently, the experimental realizations of X-ray PDC to EUV[118,178–180] or to UV–visible[181] photons have been interpreted convincingly using theoretical models[178–181,226], complementary to those used for the analysis of optical/X-ray SFG and DFG. The advent of XFELs also initiated theoretical work aimed at interpreting the first results, essentially on the multiphoton processes in atoms, yielding good agreement with experiments[122,131,134,227–230].

Theoretical efforts have been made over the past 10–15 years to explore and propose new experiments that can exploit the capabilities of XFEL and HHG sources. Some of these are discussed in the next section. The success of optical/X-ray SFG[177] at an XFEL prompted renewed theoretical activity in this area, including the development of a general theoretical framework for the interaction of general Floquet systems with an X-ray pulse[125,126,231,232]. The Floquet theory is used to describe non-perturbatively the laser-driven electronic system. The scattering probability of an arbitrary non-resonant X-ray pulse from such a system is obtained using the density-matrix formalism. These studies show how the time-dependent electron density of a crystal can be reconstructed from energy-resolved scattering patterns.

Careful inspection of the multipoint correlation functions appearing in the expression of time-resolved X-ray diffraction signals shows that diffraction also occurs from coherences on top of the usual population contributions[233,234]. The diffraction from coherences is usually neglected because it does not scale with the total number of electrons in the system, but rather depends on the few electrons involved in an optical transition. However, it is of interest to extract the coherence terms from the signal because they contain direct information on the motion of the charges at any given time. These provide new signatures of elementary dynamic phenomena in molecules and solids[227,228,235–241] such as electronic coherence created at conical intersections[242], evolving electron and nuclear densities and structural changes.

The simplest way to access these phenomena is to perturbatively disturb the molecular system with an optical field, and, at the first order in this actinic field, this corresponds to a two-point correlation function of a dipole operator and the charge density operator. Because the charge density interacts with the square of the field vector potential, the signal is reminiscent of an SFG process from the field perspective, and is therefore named X-ray sum frequency diffraction[240]. In a more general perspective, the actinic excitation can be treated non-perturbatively, typically numerically, leading to the more general ultrafast X-ray diffraction signal of non-equilibrium states that is only accessible by ultrabright, femtosecond XFEL pulses[23].

Using real-time time-dependent density functional theory simulations, DFG has been extended to the resonant case (known as resonant-DFG or re-DFG) in core transitions of specific atoms in a molecular system[123,124]. Compared with the third-order stimulated Raman process, re-DFG is a parametric process and therefore does not excite the molecule. The expected re-DFG signal strength is estimated to be stronger than the competing stimulated Raman process.

Outlook

The aforementioned survey of ultrafast EUV/X-ray nonlinear theoretical and experimental techniques shows the rich perspectives they offer in terms of fundamental science and possible applications. In the following, we discuss upcoming technical, methodological and theoretical developments and how they can shape the future of the field.

Source and method development

Sources. As for the optical domain, the development of nonlinear EUV/X-ray science has been enabled by and will expand hand-in-hand

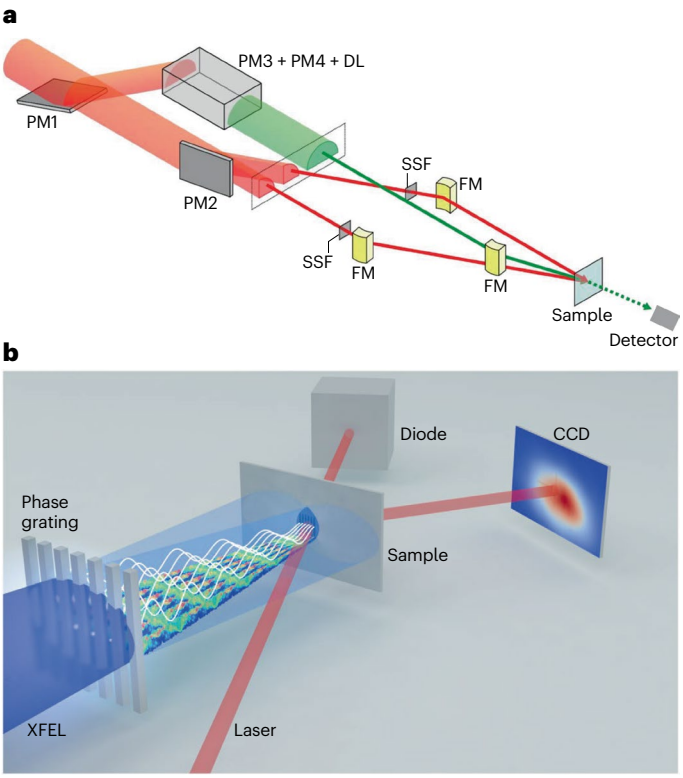

Fig. 5 | Experimental set-ups for extreme-ultraviolet/X-ray transient grating. **a**, Principle of the split-and-delay scheme used for the all-extreme-ultraviolet transient grating experiment at FERMI. The incident pulse (red) is split using plane mirrors (PM1, PM2) and, passing via solid-state filters (SSFs) and focusing mirrors (FMs), is used to excite the sample. The probe beam (green) is deflected and time-delayed using a set of adjustable plane mirrors (PM3 and PM4, with a delay line, DL) before being also sent on to the sample. **b**, In this X-ray free-electron laser (XFEL) scheme, on the basis the Talbot effect, the hard X-ray transient grating is probed by an optical pulse (red) and excitations detected using a charge-coupled-device (CCD) camera. Part **a** reprinted with permission from ref. 195, AAAS; part **b** reprinted from ref. 202, Springer Nature Limited.

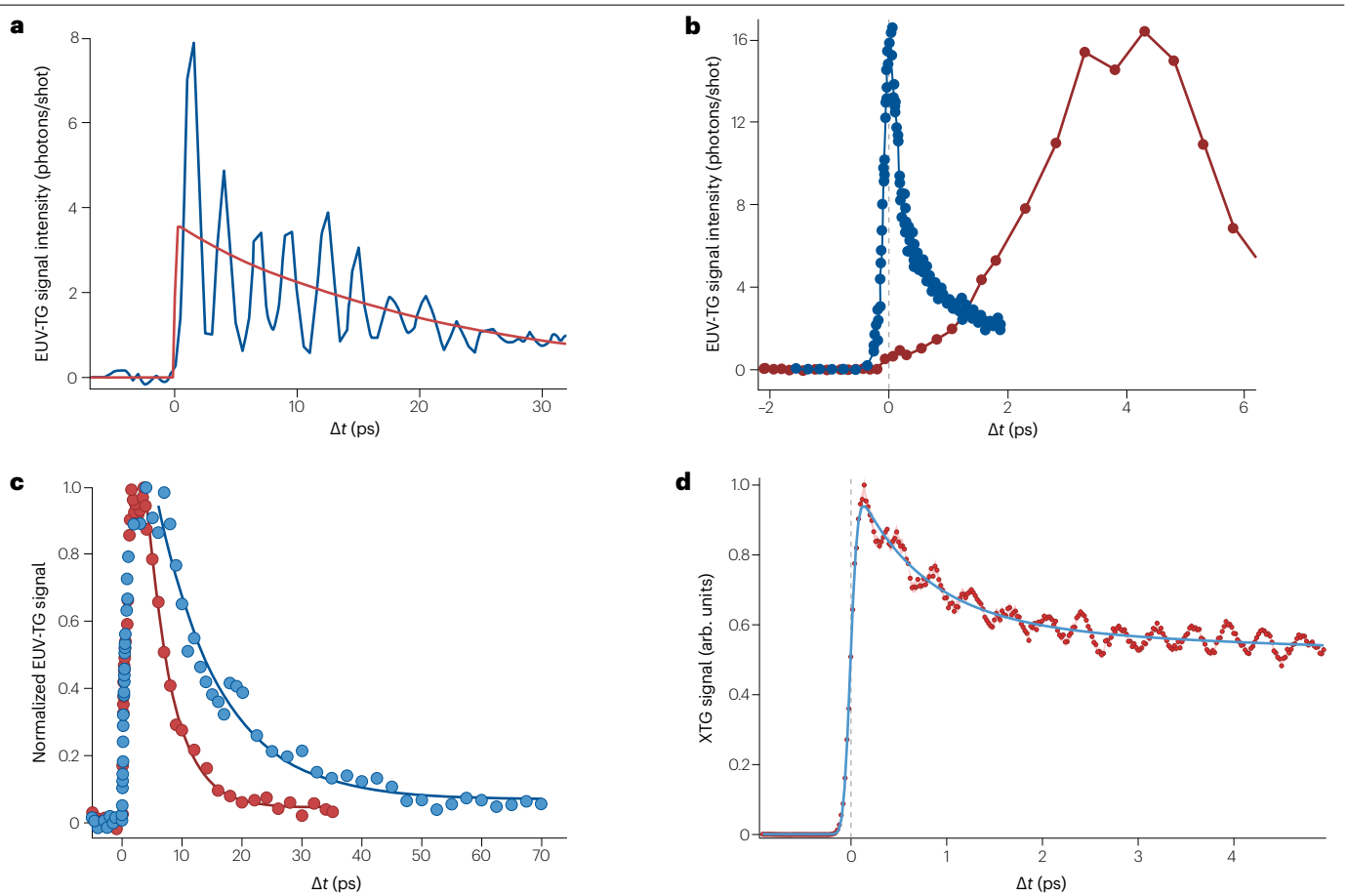

Fig. 6 | Representative extreme-ultraviolet/X-ray transient grating signals. **a**, The signal intensity for all-extreme-ultraviolet (EUV) transient grating (TG) (both pump and probe have a wavelength of 13.3 nm) on a sample of Si_3N_4 is shown as a function of the time delay Δt (between excitation and probe) for the TG period L_{TG} = 28 nm. At $\Delta t < 0$, the signal is absent because there is no grating in the sample to diffract the probe beam. The signal appears after $\Delta t = 0$ and exhibits coherent phonon oscillations (at the wavelength L_{TG}) on top of a component that is slowly decaying (red line) via thermal transport[196,310]. **b**, Early time response of the all-EUV-TG signal for L_{TG} = 85 nm (black dots) and the EUV-TG signal probed by optical pulses (blue dots, L_{TG} = 280 nm)[193,195]. The much slower rise of the all-EUV-TG signal depends on L_{TG}. The maximum signal is delayed by one-half of the acoustic oscillations period, indicating that the dominant contribution to the signal originates from density changes. **c**, L_{TG} dependence of the all-EUV-TG magnetization signal of a 9-nm-thick film of $Co_{0.81}Gd_{0.19}$ deposited on a silicon nitride membrane and probed at the $M_{2,3}$-edge of Co (59.6 eV/20.8 nm): shown for L_{TG} = 43.6 nm (yellow circles) and L_{TG} = 87.2 nm (blue circles). In both cases, the external magnetic field was 40 mT. Solid lines are exponential fits with an offset correction. **d**, Hard X-ray TG signal of bismuth germanate at 7.1 keV (L_{TG} = 770 nm), probed at 400 nm. Coherent optical phonon oscillations can be seen riding on an exponentially decaying signal (fitted blue line). Parts **a** and **b** reprinted with permission from ref. 195, AAAS; part **c** reprinted with permission from ref. 200, ACS; part **d** reprinted from ref. 202, Springer Nature Limited.

with instrumentation. In return, the drive for nonlinear science is motivating several upgrades to existing XFELs, aimed at improving the emitted pulse features: ranging from time duration to spectral purity and from repetition rate to multicolour generation. Besides the external-seeding upgrades mentioned earlier, SASE FELs are moving towards self-seeding schemes[243], which provide pulses of more stable energy, and durations of hundreds of attoseconds but with random intensities[158]. The upgraded LCLS-II machine promises a major jump in capabilities owing, in particular, to an increased repetition rate (from 120 Hz to the megahertz regime), which will enhance signal-to-noise ratios.

Many of the theoretical schemes[165,168,169,244,245] proposing stimulated X-ray Raman, emission and/or multidimensional X-ray spectroscopy rely on the use of spectrally broad, attosecond pulses that would in addition need to be phase-locked and temporally controlled. Experimental demonstrations of stimulated X-ray Raman and emission spectroscopy are realizing these predictions and showing the way forward[147,170–172,246].

An important goal in broadening the use and applications of nonlinear EUV/X-ray methods is to make them more accessible by developing smaller, table-top systems. HHG sources are making progress in this respect and in terms of repetition rate and energy or pulse stability[25,27,87]. Their ultrashort duration means high peak powers, which, for example, favour second-order processes such as TPA while minimizing sample damage.

Major efforts are being made to develop compact and economic accelerators. A new technology that could reduce the size of particle accelerators is plasma wakefield acceleration[247]. Laser wakefield accelerators can sustain accelerating gradients more than three

orders of magnitude higher than those of current (radio-frequency based) accelerators and are considered an attractive option for driving compact XFELs. The realization of such devices remains a challenge owing to the relatively poor quality of electron beams from a laser wakefield accelerator. Nevertheless, amplified undulator radiation at 27 nm has been reported with around 10^{10} photons per pulse[248], and infrared FEL radiation with the typical exponential growth of its energy over six consecutive undulators has been demonstrated[249]. Compared with SASE, the seeded FEL pulses have energies two orders of magnitude larger and a three-times-higher stability. The seeded configuration was also demonstrated at 270 nm with control over the radiation wavelength[250].

Pulse characterization. TG spectroscopy can also be implemented to characterize ultrashort pulses, overcoming the limitation of instrumentation electronics that are too slow. This is routinely done in the optical regime by FROG methods in which by spectrally resolving a nonlinear signal as a function of time delay, it is possible to obtain femtosecond or attosecond resolution owing to the radiation–matter interaction that provides an ultrafast 'shutter'[251]. In a recent study, transient grating-FROG was applied at FERMI[252] to measure the pulse length and coherence on a shot-to-shot basis by means of an EUV-transient grating and an optical probe on a slowly responding medium (an Si_3N_4 film) — thus not only demonstrating the applicability of the method at short wavelengths but also providing a valuable tool to characterize EUV-HHG and FEL pulses.

Multidimensional covariance signals. Most nonlinear spectroscopy protocols were originally designed for coherent, phase-controlled pulses. Although seeded FELs at EUV frequencies (such as FERMI) do provide coherent pulses[32,253,254], soft to hard X-ray FELs mostly involve noisy SASE pulses[32]. Their stochastic nature presents a bottleneck for the implementation of nonlinear spectroscopies that require reproducible, phase-controlled X-ray pulses. Correlation methods — based on, for example, a covariance analysis or ghost imaging — represent a promising route to overcoming this issue and retrieving information from noisy stochastic signals[170,255–258]. These methods exploit the fact that each measured signal is uniquely related to the FEL pulse generating it. They have been proposed to record the so-called transient ultrafast electronic coherences by attosecond stimulated X-ray Raman signals (TRUECARS) signals (which are discussed below).

Spectral covariance methods can be extended to a broad range of time-resolved X-ray signals, as long as different frequency-dispersed observables, such as the incident and transmitted pulse intensity profiles, can be measured and correlated. For instance, a correlation analysis of the frequency-resolved diffraction signal would enable separation of elastic and inelastic diffraction patterns and thus the imaging of the motion of electrons directly involved in the studied molecular dynamics[255]. This calls for the development of new detection methods, as well as improvements in the characterization of the X-ray pulses available at FEL sources[259,260].

Open questions and future developments

We now discuss some of the experimental and theoretical possibilities offered by nonlinear X-ray/EUV science and the questions that must be answered in order to expand the use of the methods, described above.

Surface and interface processes. There is an acute need to probe photocatalytic or electrocatalytic processes at surfaces or at buried interfaces, such as in batteries. The existing schemes[261–263] usually combine a wide variety of methods that are largely not surface- or interface-specific (ambient pressure ultraviolet or X-ray photoelectron spectroscopy, electron or X-ray diffraction, X-ray absorption or emission spectroscopy and others) making them complex and, at times, difficult to interpret. The capabilities opened up by core-level SHG, SFG and DFG (eventually combined with valence excitations for SFG and DFG) offer a unique approach to probe processes in systems such as heterojunctions and non-centrosymmetric materials with element selectivity, surface specificity, ultrahigh temporal resolution and under ambient conditions. They have the potential to become routine methods for the characterization of catalytic processes, even in the laboratory, as SHG has been demonstrated using HHG sources[87]. Such studies could be further extended to biological surfaces, for example to membranes, to probe ion exchange therein.

X-ray/optical SFG and DFG processes can be regarded as the coherently stimulated conversion of a spontaneous X-ray decay into a low-energy excited state[264] (Fig. 2a). First-order X-ray/optical mixing has been demonstrated[177], and we have indicated how another level of insight into the charge distribution can be gained by mixing the X-ray photon with one or more optical photons to generate a photon with energy that is the sum (or difference) of the energies of the incoming X-ray and optical photons[189] (Fig. 2b). Multiple Fourier components of both the first-order and second-order scattering processes (that is, for the mixing of one or two optical photons, respectively) have been calculated[265] for the optically induced charge distribution in a GaAs unit cell (Fig. 2c), indicating the feasibility of such experiments. Higher-order studies can deliver new views of functional matter, in which the dynamics of low-energy excitations determine the interaction with the environment. Applications range from information technology for data processing and storage to highly specific sensing devices.

Chirality. Chirality remains one of the most active areas in applied spectroscopy, owing to demand from the pharmaceutical and chemical industries. The most-used method is circular dichroism spectroscopy, which has intrinsically weak signals (typically 0.1% of the total absorption). Moving into the X-ray domain enhances the signals, in principle, as the higher-order terms of the Hamiltonian for light–matter interaction scale as the inverse of the radiation wavelength, and element selectivity is possible. Efforts are ongoing to implement steady-state and time-resolved linear X-ray circular dichroism (and also helical dichroism)[266–271], but further enhancements in signal intensity and selectivity could be achieved by moving to the nonlinear regime.

It was found in the 1990s that optical-domain SHG exhibits large chiral-specific responses on thin films and macromolecular assemblies[272–276]. Furthermore, theoretical and experimental studies have confirmed the viability of detectable SFG signals in isotropic chiral media[277–281]. Implementing X-ray SHG and optical/EUV or optical/X-ray SFG and DFG would provide a further degree of selectivity both on the optical side (vibrational or electronic excitations) and the EUV/X-ray side (core transitions).

Chiral crystals have a lattice structure with a well-defined handedness owing to the lack of inversion, mirror-plane or other roto-inversion symmetries. They are often topological solids in that the bulk is insulating, whereas the surface is conducting. Their electronic structure is the subject of intense investigations[282–284], but remains largely uncharacterized. Using optical/EUV or optical/X-ray SFG and DFG with circularly polarized pulses would help unravel their topological electronic properties, in particular when it comes to higher-fold chiral fermions[284].

In parallel, theoretical developments are needed to properly describe their electronic structure.

In the mid-1990s, Masahide Terazima proposed using a TG to enhance the detection of circular dichroism[285]. His idea was to use two beams that are linearly polarized at 90° to each other which creates a circularly polarized excitation grating that can then be detected background-free by a third probe pulse. Furthermore, only the difference in absorption is detected as the TG signal. Recent developments in the fields of EUV/X-ray chirality[270,271,285,286] and EUV/X-ray TG spectroscopy [193,200,202,287] suggest promising prospects for such studies[288]. In addition, nonlinear chiral signals offer a way to control which chiral pathway contributes to the final signals by using various polarization and pulse-geometry configurations[289]. X-ray Raman optical activity can be considered a fourth-order nonlinear process, involving two interactions with the incoming beam and two interactions with the spontaneously emitted photons[286]. When four classical fields are involved, it is possible to design a large class of chiral X-ray FWM techniques[288,289]: numerous pseudoscalars can be constructed from four-point-correlation functions and the irreducible tensor formalism proves useful to categorize the set of all independent combinations of incoming beam polarizations needed to extract them. Such techniques combine the advantages of nonlinear X-ray techniques such as stimulated X-ray scattering (for example, probing a large manifold of states using a single technique) with the sensitivity of inversion breaking of chiral signals.

Conical intersections. As already discussed, using stimulated X-ray Raman and X-ray emission, signal levels can be substantially enhanced owing, in particular, to the formation of a directed emitted beam that carries all the information and that can be very efficiently detected background-free. Furthermore, attosecond pulses from XFELs make it possible to beat the core-hole lifetime and further enhance the stimulated signals. Such experiments could thus preserve the high information content of RIXS, but the higher signal levels enable access to new parameter spaces (such as external fields, chemical compositions and pressure) in which systematic studies have been inhibited by the required long acquisition times. New schemes are being imagined to exploit these stimulated signals in order to address outstanding scientific questions.

An elementary molecular process that has received much attention is the passage through conical intersections: when the adiabatic states become degenerate, electronic and nuclear motions become strongly coupled, which opens ultrafast, non-radiative relaxation channels that can either go back to the reactant geometry or lead to photochemical pathways that generate new products, otherwise not accessible in the electronic ground state. Ultrafast conical intersections thus determine the outcome of photo-induced processes, such as the primary event of vision[290,291] and the photostability of DNA nucleobases against ultraviolet radiation[292]. Their spectroscopic detection remains a formidable challenge because it requires precise temporal resolution and a broad, few-electronvolt observation bandwidth. Ultrafast X-ray absorption or emission spectroscopy have been proposed as tools for their detection[241,293–296], such that the temporal and spectral profiles of the conical-intersection passage are read off by the changes in the absorption or emission lines, with the pump–probe delay encoding the dynamics of the system. Efforts are ongoing in this direction[69,297,298].

Also proposed is a probe of electronic coherence emerging at conical intersections, denoted TRUECARS[237,239,244]. Here, the X-ray probe pulse is tuned off-resonance with any material transition, and a stimulated Raman process between electronic states is induced. No probe photon is absorbed, but the spectrally dispersed probe pulse exhibits an energy redistribution on interaction with the molecule, stemming from Stokes and anti-Stokes Raman processes and leading to characteristic gain and loss features in different spectral regions. This signal requires the electronic states to be in a coherent superposition, facilitated by conical intersections through wave-packet bifurcation and subsequent population of both electronic states. The signal is background-free from state populations that dominate the transient absorption signal and it provides an unambiguous and direct probe of conical intersections. It has been proposed for the monitoring of conical intersections in nucleobases[237,299], bichromophoric molecules[233] and dendrimers[300].

The aforementioned multidimensional covariance is exemplified in TRUECARS, which requires phase-controlled pulses, but it would be similarly applicable for other frequency-resolved signals. For stochastic FEL pulses lacking phase control, the TRUECARS averaged over independent repeated measurements are expected to vanish. However, spectrally and temporally resolved information can be retrieved by an analysis of the spectral covariance between the signal and the incident pulse intensity. This two-frequency covariance map provides information by exploiting the correlations between the spectral components of the stochastic pulse, and for TRUECARS it offers the same depth of physical information that could be obtained using phase-controlled pulses[244]. The implementation of covariance methods at FELs requires knowledge of the correlation properties of the field, such as the n-point spectral correlation functions[259].

Nanoscale transport. EUV-TG methods are now well-established tools to probe the lattice, electronic and magnetic dynamics of materials. The ability to tune the grating period offers a window of opportunity for the study of various nanoscale to mesoscale transport phenomena, provided that an all-EUV geometry is used[195]. The nanoscale is hard to reach using present techniques, except in a few rare cases[301] — however, the demonstration of hard X-ray TG[202,203] opens it up, provided an all-X-ray TG configuration is adopted. This capability is being expanded to probe nanometre grating periods with adequate resolution. Recent data from experiments at SACLA and LCLS are being analysed. The extension of hard X-ray TG spectroscopy to (bio)chemical systems would offer access to short-range electron-[109] and energy-transfer[302–304] processes in biosystems as well as to chemical dynamics and diffusion in solutions. Indeed, in order to study diffusion, an experiment was carried out at the SwissFEL making a TG at the Fe K-edge of ferrioxalate in an aqueous solution[75], which was probed with 800-nm and 400-nm pulses. Further extensions into the all hard X-ray TG spectroscopy are envisaged.

The full exploitation of short-wavelength TG techniques calls, however, for a convincing demonstration of its element specificity. This is also a necessary condition for the extension of EUV/X-ray TG to multidimensional spectroscopies. Studies reporting effects owing to specific core-transition edges[198] reflect the increased absorption coefficient at the edge, but no genuine dynamics launched via excitation of specific atoms has so far been reported. A corollary to this issue is the description of the generation mechanism of the excitation. The EUV-TG generated optical phonons of bismuth germanate[196] at 2.7 THz were similarly observed in a hard X-ray transient grating experiment[202] (Fig. 6d) and, in optical impulsive stimulated Raman scattering experiments[204], and were attributed to a displacive excitation[305]. The fact that they appear in all three types of experiments calls for an understanding of the

generation mechanism of these phonons if one wants to exploit EUV or X-ray TG techniques for manipulating and controlling the dynamic properties of materials.

EUV-TG spectroscopy is the analogue of a time-domain EUV Brillouin scattering experiment. As such, EUV-TG experiments can fill the gap between optical and X-ray or neutron Brillouin scattering (Fig. 4). All-EUV-TG spectroscopy has high potential to be developed into a characterization tool — such as for nanoscale thermal transport, up to the Brillouin zone boundaries, in semiconductors and nano-devices — directly measuring the phonon mean-free-path, demagnetization dynamics of ferromagnets, collective dynamics of disordered systems (glasses and liquids), disentangling the electronic-magnetic-lattice channels and more. A new area to explore at the nanoscale is supercritical fluids, and in particular, given their importance in several applications, their non-equilibrium dynamics associated with cluster transitions and density fluctuations in binary mixtures.

Multidimensional core-level spectroscopies. Finally, the availability of tunable, attosecond and time-delayed multicolour pulses at HHG and XFEL sources is opening the way for EUV/X-ray multidimensional spectroscopies that will enable the direct interrogation of different atomic centres in a system on the timescale relevant for coherent electronic processes[306]. The full understanding of the entire range of core-level nonlinear methods described earlier (stimulated Raman[171,307], stimulated emission, multiphoton absorption[135] and so on) and the establishment of element specificity in TG experiments[195] are all ingredients necessary for the development of multidimensional core-level spectroscopies in which the crosstalk between different atomic centres (such as those suspected in two-centre metal complexes[308]) can be monitored in real time. The theoretical framework for such experiments exists[175,244,245,306] and we are confident that these experiments will be realized in the near future.

Published online: 25 September 2023

References

1. Kaiser, W. & Garrett, C. G. B. Two-photon excitation in CaF_2:Eu^{2+}. *Phys. Rev. Lett.* **7**, 229–231 (1961).
2. Franken, P. A., Hill, A. E., Peters, C. W. & Weinreich, G. Generation of optical harmonics. *Phys. Rev. Lett.* **7**, 118–119 (1961).
3. Bloembergen, N. Nonlinear optics and spectroscopy. *Rev. Mod. Phys.* **54**, 685–695 (1982).
4. Mukamel, S. *Principles of Nonlinear Optical Spectroscopy* (Oxford Univ. Press, 1995).
5. Munn, R. W. & Ironside, C. N. *Principles and Applications of Nonlinear Optical Materials* (Springer Netherlands, 1993).
6. Busch, G. E., Jones, R. P. & Rentzepis, P. M. Picosecond spectroscopy using a picosecond continuum. *Chem. Phys. Lett.* **18**, 178–185 (1973).
7. Eisenthal, K. B. Picosecond relaxation processes in chemistry. In *Ultrashort Light Pulses: Picosecond Techniques and Applications* (ed. Shapiro, S. L.) 275–315 (Springer, 1977).
8. Shank, C., Ippen, E. & Bersohn, R. Time-resolved spectroscopy of hemoglobin and its complexes with subpicosecond optical pulses. *Science* **193**, 50 (1976).
9. Zewail, A. H. Femtochemistry: atomic-scale dynamics of the chemical bond using ultrafast lasers (Nobel Lecture). *Angew. Chem. Int. Ed.* **39**, 2586–2631 (2000).
10. Ackermann, W. et al. Operation of a free-electron laser from the extreme ultraviolet to the water window. *Nat. Photon.* **1**, 336–342 (2007).
11. Allaria, E. et al. The FERMI@ Elettra free-electron-laser source for coherent X-ray physics: photon properties, beam transport system and applications. *N. J. Phys.* **12**, 075002 (2010).
12. Emma, P. et al. First lasing and operation of an angstrom-wavelength free-electron laser. *Nat. Photon.* **4**, 641–647 (2010).
13. Ishikawa, T. et al. A compact X-ray free-electron laser emitting in the sub-angstrom region. *Nat. Photon.* **6**, 540–544 (2012).
14. Prat, E. et al. A compact and cost-effective hard X-ray free-electron laser driven by a high-brightness and low-energy electron beam. *Nat. Photon.* **14**, 748–754 (2020).
15. Lappas, D. G. & L'Huillier, A. Generation of attosecond XUV pulses in strong laser-atom interactions. *Phys. Rev. A* **58**, 4140–4146 (1998).
16. Corkum, P. B., Burnett, N. H. & Ivanov, M. Y. Subfemtosecond pulses. *Opt. Lett.* **19**, 1870–1872 (1994).
17. Drescher, M. et al. X-ray pulses approaching the attosecond frontier. *Science* **291**, 1923–1927 (2001).
18. Christov, I. P., Murnane, M. M. & Kapteyn, H. C. High-harmonic generation of attosecond pulses in the 'single-cycle' regime. *Phys. Rev. Lett.* **78**, 1251–1254 (1997).
19. Chang, Z. H., Rundquist, A., Wang, H. W., Murnane, M. M. & Kapteyn, H. C. Generation of coherent soft X rays at 2.7 nm using high harmonics. *Phys. Rev. Lett.* **79**, 2967–2970 (1997).
20. Hentschel, M. et al. Attosecond metrology. *Nature* **414**, 509–513 (2001).
21. Lenzner, M., Schnurer, M., Spielmann, C. & Krausz, F. Extreme nonlinear optics with few-cycle laser pulses. *IEICE Trans. Electron.* **E81C**, 112–122 (1998).
22. Milne, C. J., Penfold, T. J. & Chergui, M. Recent experimental and theoretical developments in time-resolved X-ray spectroscopies. *Coord. Chem. Rev.* **277**, 44–68 (2014).
23. Chergui, M. & Collet, E. Photoinduced structural dynamics of molecular systems mapped by time-resolved X-ray methods. *Chem. Rev.* **117**, 11025–11065 (2017).
24. Kraus, P. M., Zürch, M., Cushing, S. K., Neumark, D. M. & Leone, S. R. The ultrafast X-ray spectroscopic revolution in chemical dynamics. *Nat. Rev. Chem.* **2**, 82–94 (2018).
25. Zong, A., Nebgen, B. R., Lin, S.-C., Spies, J. A. & Zuerch, M. Emerging ultrafast techniques for studying quantum materials. *Nat. Rev. Mater.* https://doi.org/10.1038/s41578-022-00530-0 (2023).
26. Rohringer, N. X-ray Raman scattering: a building block for nonlinear spectroscopy. *Philos. Trans. R. Soc. Math. Phys. Eng. Sci.* **377**, 20170471 (2019).
27. Leone, S. R. & Neumark, D. M. Probing matter with nonlinear spectroscopy. *Science* **379**, 536–537 (2023).
28. Khan, S. Free-electron lasers. *J. Mod. Opt.* **55**, 3469–3512 (2008).
29. Schoenlein, R. et al. Recent advances in ultrafast X-ray sources. *Philos. Trans. R. Soc. Math. Phys. Eng. Sci.* **377**, 20180384 (2019).
30. Biegert, J., Calegari, F., Dudovich, N., Quéré, F. & Vrakking, M. Attosecond technology(ies) and science. *J. Phys. B Mol. Opt. Phys.* **54**, 070201 (2021).
31. Huang, N., Deng, H., Liu, B., Wang, D. & Zhao, Z. Features and futures of X-ray free-electron lasers. *Innovation* **2**, 100097 (2021).
32. Pellegrini, C., Marinelli, A. & Reiche, S. The physics of X-ray free-electron lasers. *Rev. Mod. Phys.* **88**, 015006 (2016).
33. Margaritondo, G. & Rafelski, J. The relativistic foundations of synchrotron radiation. *J. Synchrotron Radiat.* **24**, 898–901 (2017).
34. Kondratenko, A. M. & Saldin, E. L. Generation of coherent radiation by a relativistic electron beam in an ondulator. *Part. Accel.* **10**, 207–216 (1980).
35. Allaria, E. et al. Highly coherent and stable pulses from the FERMI seeded free-electron laser in the extreme ultraviolet. *Nat. Photon.* **6**, 699–704 (2012).
36. Abela, R. et al. Perspective: opportunities for ultrafast science at SwissFEL. *Struct. Dyn.* **4**, 061602 (2017).
37. Altarelli, M., Brinkmann, R. & Chergui, M. *The European X-ray Free-electron Laser* (DESY, 2007).
38. Tschentscher, T. et al. Photon beam transport and scientific instruments at the European XFEL. *Appl. Sci.* **7**, 592 (2017).
39. Kang, H.-S. et al. Hard X-ray free-electron laser with femtosecond-scale timing jitter. *Nat. Photon.* **11**, 708–713 (2017).
40. Yu, L.-H. et al. High-gain harmonic-generation free-electron laser. *Science* **289**, 932–934 (2000).
41. Allaria, E. et al. Two-stage seeded soft-X-ray free-electron laser. *Nat. Photon.* **7**, 913–918 (2013).
42. Rebernik Ribič, P. et al. Coherent soft X-ray pulses from an echo-enabled harmonic generation free-electron laser. *Nat. Photon.* **13**, 555–561 (2019).
43. Gianessi, L. & Masciovecchio, C. (eds) *FERMI 2.0 Conceptual Design Report* (Elettra Sincrotrone Trieste, 2022); https://www.elettra.eu/images/Documents/FERMI%20Machine/Machine/CDR/FERMI2.0CDR.pdf
44. McPherson, A. et al. Studies of multiphoton production of vacuum-ultraviolet radiation in the rare gases. *J. Opt. Soc. Am. B* **4**, 595–601 (1987).
45. Ferray, M. et al. Multiple-harmonic conversion of 1064 nm radiation in rare gases. *J. Phys. B Mol. Opt. Phys.* **21**, L31–L35 (1988).
46. Corkum, P. B. & Krausz, F. Attosecond science. *Nat. Phys.* **3**, 381–387 (2007).
47. DiChiara, A. D. et al. Scaling of high-order harmonic generation in the long wavelength limit of a strong laser field. *IEEE J. Sel. Top. Quantum Electron.* **18**, 419–433 (2012).
48. Cousin, S. L. et al. High-flux table-top soft X-ray source driven by sub-2-cycle, CEP stable, 1.85-μm 1-kHz pulses for carbon K-edge spectroscopy. *Opt. Lett.* **39**, 5383–5386 (2014).
49. Kleine, C. et al. Soft X-ray absorption spectroscopy of aqueous solutions using a table-top femtosecond soft X-ray source. *J. Phys. Chem. Lett.* **10**, 52–58 (2019).
50. Chang, Z. Enhancing keV high harmonic signals generated by long-wave infrared lasers. *OSA Contin.* **2**, 2131–2136 (2019).
51. Kroh, T. et al. Enhanced high-harmonic generation up to the soft X-ray region driven by mid-infrared pulses mixed with their third harmonic. *Opt. Express* **26**, 16955–16969 (2018).
52. Makos, I. et al. A 10-gigawatt attosecond source for non-linear XUV optics and XUV-pump-XUV-probe studies. *Sci. Rep.* **10**, 3759 (2020).
53. Pupeza, I. et al. Compact high-repetition-rate source of coherent 100 eV radiation. *Nat. Photon.* **7**, 608–612 (2013).
54. Hädrich, S. et al. Exploring new avenues in high repetition rate table-top coherent extreme ultraviolet sources. *Light Sci. Appl.* **4**, e320–e320 (2015).
55. Rossi, G. M. et al. Sub-cycle millijoule-level parametric waveform synthesizer for attosecond science. *Nat. Photon.* **14**, 629–635 (2020).

56. Geneaux, R., Marroux, H. J. B., Guggenmos, A., Neumark, D. M. & Leone, S. R. Transient absorption spectroscopy using high harmonic generation: a review of ultrafast X-ray dynamics in molecules and solids. *Philos. Trans. R Soc. Math. Phys. Eng. Sci.* **377**, 20170463 (2019).
57. Park, J., Subramani, A., Kim, S. & Ciappina, M. F. Recent trends in high-order harmonic generation in solids. *Adv. Phys. X* **7**, 2003244 (2022).
58. Luu, T. T. et al. Extreme–ultraviolet high-harmonic generation in liquids. *Nat. Commun.* **9**, 3723 (2018).
59. Zeng, A.-W. & Bian, X.-B. Impact of statistical fluctuations on high harmonic generation in liquids. *Phys. Rev. Lett.* **124**, 203901 (2020).
60. Agostini, P. & DiMauro, L. F. The physics of attosecond light pulses. *Rep. Prog. Phys.* **67**, 813–855 (2004).
61. Gallmann, L., Cirelli, C. & Keller, U. Attosecond science: recent highlights and future trends. *Annu. Rev. Phys. Chem.* **63**, 447–469 (2012).
62. Krausz, F. & Ivanov, M. Attosecond physics. *Rev. Mod. Phys.* **81**, 163 (2009).
63. Frank, F. et al. Invited review article: technology for attosecond science. *Rev. Sci. Instrum.* **83**, 071101 (2012).
64. Boutu, W., Ducousso, M., Hergott, J.-F. & Merdji, H. Overview on HHG high-flux sources. in *Optical Technologies for Extreme-Ultraviolet and Soft X-ray Coherent Sources* (eds Canova, F. & Poletto, L.) 63–78 (Springer, 2015).
65. Franz, D. et al. All semiconductor enhanced high-harmonic generation from a single nanostructured cone. *Sci. Rep.* **9**, 5663 (2019).
66. Jürgens, P. et al. Origin of strong-field-induced low-order harmonic generation in amorphous quartz. *Nat. Phys.* **16**, 1035–1039 (2020).
67. Gholam-Mirzaei, S., Beetar, J. E., Chacón, A. & Chini, M. High-harmonic generation in ZnO driven by self-compressed mid-infrared pulses. *J. Opt. Soc. Am. B* **35**, A27–A31 (2018).
68. Pertot, Y. et al. Time-resolved X-ray absorption spectroscopy with a water window high-harmonic source. *Science* **355**, 264–267 (2017).
69. Zinchenko, K. S. et al. Sub-7-femtosecond conical-intersection dynamics probed at the carbon K-edge. *Science* **371**, 489–494 (2021).
70. Gallmann, L. et al. Photoemission and photoionization time delays and rates. *Struct. Dyn.* **4**, 061502 (2017).
71. Faccialà, D. et al. Time-resolved chiral X-ray photoelectron spectroscopy with transiently enhanced atomic site-selectivity: a free electron laser investigation of electronically excited fenchone enantiomers. *Phys. Rev. X* **13**, 011044 (2022).
72. Wörner, H. J., Bertrand, J. B., Kartashov, D. V., Corkum, P. B. & Villeneuve, D. M. Following a chemical reaction using high-harmonic interferometry. *Nature* **466**, 604–607 (2010).
73. Abel, B., Buck, U., Sobolewski, A. L. & Domcke, W. On the nature and signatures of the solvated electron in water. *Phys. Chem. Chem. Phys.* **14**, 22–34 (2012).
74. Hummert, J. et al. Femtosecond extreme ultraviolet photoelectron spectroscopy of organic molecules in aqueous solution. *J. Phys. Chem. Lett.* **9**, 6649–6655 (2018).
75. Longetti, L. et al. Ultrafast photoelectron spectroscopy of photoexcited aqueous ferrioxalate. *Phys. Chem. Chem. Phys.* **23**, 25308–25316 (2021).
76. Arrell, C. A. et al. Laser-assisted photoelectric effect from liquids. *Phys. Rev. Lett.* **117**, 143001 (2016).
77. Crepaldi, A. et al. Time-resolved ARPES at LACUS: band structure and ultrafast electron dynamics of solids. *CHIMIA* **71**, 273–277 (2017).
78. Gatti, G. et al. Light-induced renormalization of the Dirac quasiparticles in the nodal-line semimetal ZrSiSe. *Phys. Rev. Lett.* **125**, 076401 (2020).
79. Fidler, A. P. et al. Nonlinear XUV signal generation probed by transient grating spectroscopy with attosecond pulses. *Nat. Commun.* **10**, 1384 (2019).
80. Grilj, J. et al. Self referencing heterodyne transient grating spectroscopy with short wavelength. *Photonics* **2**, 392–401 (2015).
81. Cao, W., Warrick, E. R., Fidler, A., Neumark, D. M. & Leone, S. R. Noncollinear wave mixing of attosecond XUV and few-cycle optical laser pulses in gas-phase atoms: toward multidimensional spectroscopy involving XUV excitations. *Phys. Rev. A* **94**, 053846 (2016).
82. Mairesse, Y. et al. High-order harmonic transient grating spectroscopy in a molecular jet. *Phys. Rev. Lett.* **100**, 143903 (2008).
83. Ruf, H. et al. High-harmonic transient grating spectroscopy of NO_2 electronic relaxation. *J. Chem. Phys.* **137**, 224303 (2012).
84. Orfanos, I. et al. Non-linear processes in the extreme ultraviolet. *J. Phys. Photon.* **2**, 042003 (2020).
85. Senfftleben, B. et al. Highly non-linear ionization of atoms induced by intense high-harmonic pulses. *J. Phys. Photon.* **2**, 034001 (2020).
86. Drescher, L. et al. Extreme-ultraviolet spectral compression by four-wave mixing. *Nat. Photon.* **15**, 263–266 (2021).
87. Helk, T. et al. Table-top extreme ultraviolet second harmonic generation. *Sci. Adv.* **7**, eabe2265 (2021).
88. Shen, Y. R. *Principles of Nonlinear Optics* (U.S. Department of Energy, 1984).
89. Boyd, R. W. *Nonlinear Optics* (Academic Press, 2020).
90. Corn, R. M. & Higgins, D. A. Optical second harmonic generation as a probe of surface chemistry. *Chem. Rev.* **94**, 107–125 (1994).
91. Shi, X., Borguet, E., Tarnovsky, A. N. & Eisenthal, K. B. Ultrafast dynamics and structure at aqueous interfaces by second harmonic generation. *Chem. Phys.* **205**, 167–178 (1996).
92. Wang, H., Borguet, E. & Eisenthal, K. B. Polarity of liquid interfaces by second harmonic generation spectroscopy. *J. Phys. Chem. A* **101**, 713–718 (1997).
93. Eisenthal, K. B. Liquid interfaces probed by second-harmonic and sum-frequency spectroscopy. *Chem. Rev.* **96**, 1343–1360 (1996).
94. Almogy, G. & Yariv, A. Resonantly-enhanced nonlinear optics of intersubband transitions. *J. Nonlinear Opt. Phys. Mater.* **4**, 401–458 (1995).
95. Oudar, J.-L. & Shen, Y. R. Nonlinear spectroscopy by multiresonant four-wave mixing. *Phys. Rev. A* **22**, 1141–1158 (1980).
96. Begley, R. F., Harvey, A. B. & Byer, R. L. Coherent anti-stokes Raman spectroscopy. *Appl. Phys. Lett.* **25**, 387–390 (1974).
97. Giordmaine, J. A. Mixing of light beams in crystals. *Phys. Rev. Lett.* **8**, 19–20 (1962).
98. Jones, W. J. & Stoicheff, B. P. Inverse Raman spectra: induced absorption at optical frequencies. *Phys. Rev. Lett.* **13**, 657–659 (1964).
99. Maker, P. D. & Terhune, R. W. Study of optical effects due to an induced polarization third order in the electric field strength. *Phys. Rev.* **137**, A801–A818 (1965).
100. Duncan, M. D., Reintjes, J. & Manuccia, T. J. Scanning coherent anti-Stokes Raman microscope. *Opt. Lett.* **7**, 350–352 (1982).
101. Hofmann, F., Short, M. P. & Dennett, C. A. Transient grating spectroscopy: an ultrarapid, nondestructive materials evaluation technique. *MRS Bull.* **44**, 392–402 (2019).
102. Ernst, R. R., Bodenhausen, G. & Wokaun, A. *Principles of Nuclear Magnetic Resonance in One and Two Dimensions* Vol. 14 (Clarendon Press, 1987).
103. Mukamel, S., Tanimura, Y. & Hamm, P. Coherent multidimensional optical spectroscopy. *Acc. Chem. Res.* **42**, 1207–1209 (2009).
104. Hamm, P. & Zanni, M. *Concepts and Methods of 2D Infrared Spectroscopy* (Cambridge Univ. Press, 2011).
105. Brixner, T., Stiopkin, I. V. & Fleming, G. R. Tunable two-dimensional femtosecond spectroscopy. *Opt. Lett.* **29**, 884–886 (2004).
106. Brixner, T. et al. Two-dimensional spectroscopy of electronic couplings in photosynthesis. *Nature* **434**, 625–628 (2005).
107. Haddad, A. A. et al. Set-up for broadband Fourier-transform multidimensional electronic spectroscopy. *Opt. Lett.* **40**, 312–315 (2015).
108. Auböck, G., Consani, C., Mourik, F. & Chergui, M. Ultrabroadband femtosecond two-dimensional ultraviolet transient absorption. *Opt. Lett.* **37**, 2337–2339 (2012).
109. Consani, C., Aubock, G., van Mourik, F. & Chergui, M. Ultrafast tryptophan-to-haem electron transfer in myoglobins revealed by UV 2D spectroscopy. *Science* **339**, 1586–1589 (2013).
110. Borrego-Varillas, R. et al. Two-dimensional electronic spectroscopy in the ultraviolet by a birefringent delay line. *Opt. Express* **24**, 28491–28499 (2016).
111. Freund, I. & Levine, B. F. Parametric conversion of X rays. *Phys. Rev. Lett.* **23**, 854–857 (1969).
112. Eisenberger, P. & McCall, S. L. X-ray parametric conversion. *Phys. Rev. Lett.* **26**, 684–688 (1971).
113. Eisenberger, P. M. & McCall, S. L. Mixing of X-ray and optical photons. *Phys. Rev. A* **3**, 1145–1151 (1971).
114. Woo, J. W. F. & Jha, S. S. Inelastic scattering of X rays from optically induced charge-density oscillations. *Phys. Rev. B* **6**, 4081–4082 (1972).
115. Freund, I. Nonlinear X-ray spectroscopy. *Opt. Commun.* **6**, 421–423 (1972).
116. Freund, I. & Levine, B. F. Surface effects in the nonlinear interaction of X-ray and optical fields. *Phys. Rev. B* **8**, 3059–3060 (1973).
117. Flytzanis, C. Determination of local field in dielectric. *C. R. Acad. Sci. Serie B* **278**, 339–342 (1975).
118. Danino, H. & Freund, I. Parametric down conversion of X rays into the extreme ultraviolet. *Phys. Rev. Lett.* **46**, 1127–1130 (1981).
119. Tanaka, S., Chernyak, V. & Mukamel, S. Time-resolved X-ray spectroscopies: nonlinear response functions and Liouville-space pathways. *Phys. Rev. A* **63**, 063405 (2001).
120. Tanaka, S. & Mukamel, S. Coherent X-ray Raman spectroscopy: a nonlinear local probe for electronic excitations. *Phys. Rev. Lett.* **89**, 043001 (2002).
121. Tanaka, S. & Mukamel, S. X-ray four-wave mixing in molecules. *J. Chem. Phys.* **116**, 1877–1891 (2002).
122. Doumy, G. et al. Nonlinear atomic response to intense ultrashort X rays. *Phys. Rev. Lett.* **106**, 083002 (2011).
123. Serrat, C. Localized core four-wave mixing buildup in the X-ray spectrum of chemical species. *J. Phys. Chem. Lett.* **12**, 1093–1097 (2021).
124. Serrat, C. Resonantly enhanced difference-frequency generation in the core X-ray absorption of molecules. *J. Phys. Chem. A* **125**, 10706–10710 (2021).
125. Haber, J. et al. Nonlinear resonant X-ray Raman scattering. Preprint at https://doi.org/10.48550/arXiv.2006.14724 (2020).
126. Popova-Gorelova, D., Reis, D. A. & Santra, R. Theory of X-ray scattering from laser-driven electronic systems. *Phys. Rev. B* **98**, 224302 (2018).
127. Misoguti, L., Christov, I. P., Backus, S., Murnane, M. M. & Kapteyn, H. C. Nonlinear wave-mixing processes in the extreme ultraviolet. *Phys. Rev. A* **72**, 063803 (2005).
128. Maznev, A. A., Nelson, K. A. & Rogers, J. A. Optical heterodyne detection of laser-induced gratings. *Opt. Lett.* **23**, 1319–1321 (1998).
129. Katayama, K., Yamaguchi, M. & Sawada, T. Lens-free heterodyne detection for transient grating experiments. *Appl. Phys. Lett.* **82**, 2775–2777 (2003).
130. Sorokin, A. A. et al. Photoelectric effect at ultrahigh intensities. *Phys. Rev. Lett.* **99**, 213002 (2007).
131. Kanter, E. P. et al. Unveiling and driving hidden resonances with high-fluence, high-intensity X-ray pulses. *Phys. Rev. Lett.* **107**, 233001 (2011).
132. Lambropoulos, P. & Tang, X. Multiple excitation and ionization of atoms by strong lasers. *J. Opt. Soc. Am. B* **4**, 821–832 (1987).
133. Novikov, S. A. & Hopersky, A. N. Two-photon excitation-ionization of the 1s shell of highly charged positive atomic ions. *J. Phys. B Mol. Opt. Phys.* **34**, 4857–4863 (2001).

134. Sytcheva, A., Pabst, S., Son, S.-K. & Santra, R. Enhanced nonlinear response of Ne^{8+} to intense ultrafast X rays. *Phys. Rev. A* **85**, 023414 (2012).
135. Tamasaku, K. et al. X-ray two-photon absorption competing against single and sequential multiphoton processes. *Nat. Photon.* **8**, 313–316 (2014).
136. Ghimire, S. et al. Nonsequential two-photon absorption from the *K* shell in solid zirconium. *Phys. Rev. A* **94**, 043418 (2016).
137. Tamasaku, K. et al. Nonlinear spectroscopy with X-ray two-photon absorption in metallic copper. *Phys. Rev. Lett.* **121**, 083901 (2018).
138. Powers, P. E. & Haus, J. W. *Fundamentals of Nonlinear Optics* (CRC Press, 2017).
139. Paschotta, R. & Keller, U. Passive mode locking with slow saturable absorbers. *Appl. Phys. B* **73**, 653–662 (2001).
140. Wang, G. et al. Broadband saturable absorption and exciton–exciton annihilation in $MoSe_2$ composite thin films. *Opt. Mater. Express* **9**, 483–496 (2019).
141. Kumar, S. et al. Femtosecond carrier dynamics and saturable absorption in graphene suspensions. *Appl. Phys. Lett.* **95**, 191911 (2009).
142. Bob, Nagler et al. Turning solid aluminium transparent by intense soft X-ray photoionization. *Nat. Phys.* **5**, 693–696 (2009).
143. Yoneda, H. et al. Ultra-fast switching of light by absorption saturation in vacuum ultra-violet region. *Opt. Express* **17**, 23443–23448 (2009).
144. Yoneda, H. et al. Saturable absorption of intense hard X-rays in iron. *Nat. Commun.* **5**, 5080 (2014).
145. Hoffmann, L. et al. Saturable absorption of free-electron laser radiation by graphite near the carbon K-edge. *J. Phys. Chem. Lett.* **13**, 8963–8970 (2022).
146. Rohringer, N. et al. Atomic inner-shell X-ray laser at 1.46 nanometres pumped by an X-ray free-electron laser. *Nature* **481**, 488–491 (2012).
147. Beye, M. et al. Stimulated X-ray emission for materials science. *Nature* **501**, 191–194 (2013).
148. Jonnard, P. et al. EUV stimulated emission from MgO pumped by FEL pulses. *Struct. Dyn.* **4**, 054306 (2017).
149. Yoneda, H. et al. Atomic inner-shell laser at 1.5-ångström wavelength pumped by an X-ray free-electron laser. *Nature* **524**, 446–449 (2015).
150. Glatzel, P. & Bergmann, U. High resolution 1s core hole X-ray spectroscopy in 3*d* transition metal complexes — electronic and structural information. *Coord. Chem. Rev.* **249**, 65–95 (2005).
151. Zhang, W. et al. Tracking excited-state charge and spin dynamics in iron coordination complexes. *Nature* **509**, 345–348 (2014).
152. Kinschel, D. et al. Femtosecond X-ray emission study of the spin cross-over dynamics in haem proteins. *Nat. Commun.* **11**, 4145 (2020).
153. Bacellar, C. et al. Spin cascade and doming in ferric hemes: femtosecond X-ray absorption and X-ray emission studies. *Proc. Natl Acad. Sci. USA* **117**, 21914–21920 (2020).
154. March, A. M. et al. Probing transient valence orbital changes with picosecond valence-to-core X-ray emission spectroscopy. *J. Phys. Chem. C* **121**, 2620–2626 (2017).
155. Ledbetter, K. et al. Excited state charge distribution and bond expansion of ferrous complexes observed with femtosecond valence-to-core X-ray emission spectroscopy. *J. Chem. Phys.* **152**, 074203 (2020).
156. Kroll, T. et al. Stimulated X-ray emission spectroscopy in transition metal complexes. *Phys. Rev. Lett.* **120**, 133203 (2018).
157. Kroll, T. et al. Observation of seeded Mn Kβ stimulated X-ray emission using two-color X-ray free-electron laser pulses. *Phys. Rev. Lett.* **125**, 037404 (2020).
158. Duris, J. et al. Tunable isolated attosecond X-ray pulses with gigawatt peak power from a free-electron laser. *Nat. Photon.* **14**, 30–36 (2020).
159. McCamant, D. W., Kukura, P. & Mathies, R. A. Femtosecond stimulated Raman study of excited-state evolution in bacteriorhodopsin. *J. Phys. Chem. B* **109**, 10449–10457 (2005).
160. Kukura, P., McCamant, D. W. & Mathies, R. A. Femtosecond stimulated Raman spectroscopy. *Annu. Rev. Phys. Chem.* **58**, 461–488 (2007).
161. Hahn, A. W. et al. Probing the valence electronic structure of low-spin ferrous and ferric complexes using 2p3d resonant inelastic X-ray scattering (RIXS). *Inorg. Chem.* **57**, 9515–9530 (2018).
162. Van Kuiken, B. E. et al. Electronic spectra of iron–sulfur complexes measured by 2p3d RIXS spectroscopy. *Inorg. Chem.* **57**, 7355–7361 (2018).
163. Ågren, H., Luo, Y., Gelmukhanov, F. & Jensen, H. J. A. Screening in resonant X-ray emission of molecules. *J. Electron Spectrosc. Relat. Phenom.* **82**, 125–134 (1996).
164. Cho, D., Rouxel, J. R., Mukamel, S., Kin-Lic Chan, G. & Li, Z. Stimulated X-ray Raman and absorption spectroscopy of iron–sulfur dimers. *J. Phys. Chem. Lett.* **10**, 6664–6671 (2019).
165. Schweigert, I. V. & Mukamel, S. Probing valence electronic wave-packet dynamics by all X-ray stimulated Raman spectroscopy: a simulation study. *Phys. Rev. A* **76**, 012504 (2007).
166. Harbola, U. & Mukamel, S. Coherent stimulated X-ray Raman spectroscopy: attosecond extension of resonant inelastic X-ray Raman scattering. *Phys. Rev. B* **79**, 085108 (2009).
167. Hua, W. et al. Monitoring conical intersections in the ring opening of furan by attosecond stimulated X-ray Raman spectroscopy. *Struct. Dyn.* **3**, 023601 (2016).
168. Weninger, C. Stimulated electronic X-ray Raman scattering. *Phys. Rev. Lett.* **111**, 233902 (2013).
169. Weninger, C. & Rohringer, N. Stimulated resonant X-ray Raman scattering with incoherent radiation. *Phys. Rev. A* **88**, 053421 (2013).
170. Kimberg, V. & Rohringer, N. Stochastic stimulated electronic X-ray Raman spectroscopy. *Struct. Dyn.* **3**, 034101 (2016).
171. O'Neal, J. T. et al. Electronic population transfer via impulsive stimulated X-ray Raman scattering with attosecond soft-X-ray pulses. *Phys. Rev. Lett.* **125**, 073203 (2020).
172. Higley, D. J. et al. Stimulated resonant inelastic X-ray scattering in a solid. *Commun. Phys.* **5**, 1–12 (2022).
173. Arya, K. & Jha, S. S. Microscopic optical fields and mixing coefficients of X-ray and optical frequencies in solids. *Pramana* **2**, 116–125 (1974).
174. Pine, A. S. Self-consistent-field theory of linear and nonlinear crystalline dielectrics including local-field effects. *Phys. Rev.* **139**, A901–A911 (1965).
175. Schweigert, I. V. & Mukamel, S. Coherent ultrafast core-hole correlation spectroscopy: X-ray analogues of multidimensional NMR. *Phys. Rev. Lett.* **99**, 163001 (2007).
176. Nazarkin, A., Podorov, S., Uschmann, I., Förster, E. & Sauerbrey, R. Nonlinear optics in the angstrom regime: hard-X-ray frequency doubling in perfect crystals. *Phys. Rev. A* **67**, 041804 (2003).
177. Glover, T. E. et al. X-ray and optical wave mixing. *Nature* **488**, 603–608 (2012).
178. Tamasaku, K. & Ishikawa, T. Interference between Compton scattering and X-ray parametric down-conversion. *Phys. Rev. Lett.* **98**, 244801 (2007).
179. Tamasaku, K., Sawada, K. & Ishikawa, T. Determining X-ray nonlinear susceptibility of diamond by the optical Fano effect. *Phys. Rev. Lett.* **103**, 254801 (2009).
180. Tamasaku, K., Sawada, K., Nishibori, E. & Ishikawa, T. Visualizing the local optical response to extreme-ultraviolet radiation with a resolution of λ/380. *Nat. Phys.* **7**, 705–708 (2011).
181. Schori, A. et al. Parametric down-conversion of X rays into the optical regime. *Phys. Rev. Lett.* **119**, 253902 (2017).
182. Shwartz, S. et al. X-ray second harmonic generation. *Phys. Rev. Lett.* **112**, 163901 (2014).
183. Lam, R. K. et al. Soft X-ray second harmonic generation as an interfacial probe. *Phys. Rev. Lett.* **120**, 023901 (2018).
184. Yamamoto, S. et al. Element selectivity in second-harmonic generation of $GaFeO_3$ by a soft-X-ray free-electron laser. *Phys. Rev. Lett.* **120**, 223902 (2018).
185. Berger, E. et al. Extreme ultraviolet second harmonic generation spectroscopy in a polar metal. *Nano Lett.* **21**, 6095–6101 (2021).
186. Schwartz, C. P. et al. Angstrom-resolved interfacial structure in buried organic–inorganic junctions. *Phys. Rev. Lett.* **127**, 096801 (2021).
187. Sistrunk, E. et al. Extreme ultraviolet transient grating measurement of insulator–metal transition dynamics of VO_2. In *19th International Conference on Ultrafast Phenomena* (OSA, 2014); https://doi.org/10.1364/UP.2014.09.Wed.P3.44.
188. Gaynor, J. D. et al. Solid state core-exciton dynamics in NaCl observed by tabletop attosecond four-wave mixing spectroscopy. *Phys. Rev. B* **103**, 245140 (2021).
189. Rottke, H. et al. Probing electron and hole colocalization by resonant four-wave mixing spectroscopy in the extreme ultraviolet. *Sci. Adv.* **8**, eabn5127 (2022).
190. Sander, M. et al. Spatiotemporal coherent control of thermal excitations in solids. *Phys. Rev. Lett.* **119**, 075901 (2017).
191. Pudell, J.-E. et al. Full spatiotemporal control of laser-excited periodic surface deformations. *Phys. Rev. Appl.* **12**, 024036 (2019).
192. Frazer, T. D. et al. Optical transient grating pumped X-ray diffraction microscopy for studying mesoscale structural dynamics. *Sci. Rep.* **11**, 19322 (2021).
193. Bencivenga, F. et al. Four-wave mixing experiments with extreme ultraviolet transient gratings. *Nature* **520**, 205–208 (2015).
194. Foglia, L. et al. First evidence of purely extreme-ultraviolet four-wave mixing. *Phys. Rev. Lett.* **120**, 263901 (2018).
195. Bencivenga, F. et al. Nanoscale transient gratings excited and probed by extreme ultraviolet femtosecond pulses. *Sci. Adv.* **5**, eaaw5805 (2019).
196. Maznev, A. A. et al. Generation of coherent phonons by coherent extreme ultraviolet radiation in a transient grating experiment. *Appl. Phys. Lett.* **113**, 221905 (2018).
197. Maznev, A. A. et al. Generation and detection of 50 GHz surface acoustic waves by extreme ultraviolet pulses. *Appl. Phys. Lett.* **119**, 044102 (2021).
198. Bohinc, R. et al. Nonlinear XUV-optical transient grating spectroscopy at the Si L2,3-edge. *Appl. Phys. Lett.* **114**, 181101 (2019).
199. Naumenko, D. et al. Thermoelasticity of nanoscale silicon carbide membranes excited by extreme ultraviolet transient gratings: implications for mechanical and thermal management. *ACS Appl. Nano Mater.* **2**, 5132–5139 (2019).
200. Ksenzov, D. et al. Nanoscale transient magnetization gratings created and probed by femtosecond extreme ultraviolet pulses. *Nano Lett.* **21**, 2905–2911 (2021).
201. Yao, K. et al. All-optical switching on the nanometer scale excited and probed with femtosecond extreme ultraviolet pulses. *Nano Lett.* **22**, 4452–4458 (2022).
202. Rouxel, J. R. et al. Hard X-ray transient grating spectroscopy on bismuth germanate. *Nat. Photon.* **15**, 499–503 (2021).
203. Svetina, C. et al. Towards X-ray transient grating spectroscopy. *Opt. Lett.* **44**, 574–577 (2019).
204. Chen, Z., Gao, Y., Minch, B. C. & DeCamp, M. F. Coherent optical phonon generation in $Bi_3Ge_4O_{12}$. *J. Phys. Condens. Matter* **23**, 385402 (2011).
205. Peters, W. et al. Hard X-ray–optical transient grating. In *2021 Conference on Lasers and Electro-Optics* (*CLEO*) 1–2 (CLEO, 2021).
206. Shi, H. & Zhu, D. Multi-axis nanopositioning system for the hard X-ray split-delay system at the LCLS. *Synchrotron Radiat. News* **31**, 15–20 (2018).
207. Ukleev, V. et al. Effect of intense X-ray free-electron laser transient gratings on the magnetic domain structure of Tm:YIG. *J. Appl. Phys.* **133**, 123902 (2023).
208. Keefer, D. et al. Ultrafast X-ray probes of elementary molecular events. *Ann. Rev. Phys. Chem.* **74**, 73–97 (2023).
209. Roemelt, M., Maganas, D., DeBeer, S. & Neese, F. A combined DFT and restricted open-shell configuration interaction method including spin–orbit coupling: application to transition metal L-edge X-ray absorption spectroscopy. *J. Chem. Phys.* **138**, 204101 (2013).

210. Norman, P. & Dreuw, A. Simulating X-ray spectroscopies and calculating core-excited states of molecules. *Chem. Rev.* **118**, 7208–7248 (2018).
211. Vidal, M. L., Feng, X., Epifanovsky, E., Krylov, A. I. & Coriani, S. New and efficient equation-of-motion coupled-cluster framework for core-excited and core-ionized states. *J. Chem. Theory Comput.* **15**, 3117–3133 (2019).
212. Montorsi, F., Segatta, F., Nenov, A., Mukamel, S. & Garavelli, M. Soft X-ray spectroscopy simulations with multiconfigurational wave function theory: spectrum completeness, sub-eV accuracy, and quantitative reproduction of line shapes. *J. Chem. Theory Comput.* **18**, 1003–1016 (2022).
213. Tully, J. C. Molecular dynamics with electronic transitions. *J. Chem. Phys.* **93**, 1061–1071 (1990).
214. Meyer, H.-D., Manthe, U. & Cederbaum, L. S. The multi-configurational time-dependent Hartree approach. *Chem. Phys. Lett.* **165**, 73–78 (1990).
215. Ben-Nun, M. & Martinez, T. J. Ab initio quantum molecular dynamics. *Adv. Chem. Phys.* **121**, 439–512 (2002).
216. Makhov, D. V., Glover, W. J., Martinez, T. J. & Shalashilin, D. V. Ab initio multiple cloning algorithm for quantum nonadiabatic molecular dynamics. *J. Chem. Phys.* **141**, 054110 (2014).
217. Richter, M., Marquetand, P., González-Vázquez, J., Sola, I. & González, L. SHARC: ab initio molecular dynamics with surface hopping in the adiabatic representation including arbitrary couplings. *J. Chem. Theory Comput.* **7**, 1253–1258 (2011).
218. Reiter, S., Keefer, D. & de Vivie-Riedle, R. Exact quantum dynamics (wave packets) in reduced dimensionality. in *Quantum Chemistry and Dynamics of Excited States* 355–381 (John Wiley & Sons, Ltd, 2020).
219. Helmich-Paris, B. Simulating X-ray absorption spectra with complete active space self-consistent field linear response methods. *Int. J. Quantum Chem.* **121**, e26559 (2021).
220. Casanova, D. Restricted active space configuration interaction methods for strong correlation: Recent developments. *WIREs Comput Mol Sci.* **12**, e1561 (2022).
221. Autschbach, J., Ziegler, T., van Gisbergen, S. J. A. & Baerends, E. J. Chiroptical properties from time-dependent density functional theory. I. Circular dichroism spectra of organic molecules. *J. Chem. Phys.* **116**, 6930–6940 (2002).
222. Lopata, K., Van Kuiken, B. E., Khalil, M. & Govind, N. Linear-response and real-time time-dependent density functional theory studies of core-level near-edge X-ray absorption. *J. Chem. Theory Comput.* **8**, 3284–3292 (2012).
223. Andersen, J. H., Nanda, K. D., Krylov, A. I. & Coriani, S. Probing molecular chirality of ground and electronically excited states in the UV–vis and X-ray regimes: an EOM-CCSD study. *J. Chem. Theory Comput.* **18**, 1748–1764 (2022).
224. Nanda, K. D. & Krylov, A. I. Cherry-picking resolvents: a general strategy for convergent coupled-cluster damped response calculations of core-level spectra. *J. Chem. Phys.* **153**, 141104 (2020).
225. Freund, I. Nonlinear X-ray diffraction. Determination of valence electron charge distributions. *Chem. Phys. Lett.* **12**, 583–588 (1972).
226. Shwartz, E. & Shwartz, S. Difference-frequency generation of optical radiation from two-color X-ray pulses. *Opt. Express* **23**, 7471–7480 (2015).
227. Rohringer, N. & Santra, R. X-ray nonlinear optical processes using a self-amplified spontaneous emission free-electron laser. *Phys. Rev. A* **76**, 033416 (2007).
228. Santra, R., Kryzhevoi, N. V. & Cederbaum, L. S. X-ray two-photon photoelectron spectroscopy: a theoretical study of inner-shell spectra of the organic para-aminophenol molecule. *Phys. Rev. Lett.* **103**, 013002 (2009).
229. Motomura, K. et al. Sequential multiphoton multiple ionization of atomic argon and xenon irradiated by X-ray free-electron laser pulses from SACLA. *J. Phys. B Mol. Opt. Phys.* **46**, 164024 (2013).
230. Mazza, T. et al. Sensitivity of nonlinear photoionization to resonance substructure in collective excitation. *Nat. Commun.* **6**, 6799 (2015).
231. Popova-Gorelova, D., Guskov, V. & Santra, R. Microscopic electron dynamics in nonlinear optical response of solids. Preprint at https://doi.org/10.48550/arXiv.2009.07527 (2020).
232. Popova-Gorelova, D. & Santra, R. Atomic-scale imaging of laser-driven electron dynamics in solids using subcycle-resolved X-ray-optical wave mixing. Preprint at https://doi.org/10.48550/arXiv.2012.10334 (2020).
233. Keefer, D. et al. Monitoring molecular vibronic coherences in a bichromophoric molecule by ultrafast X-ray spectroscopy. *Chem. Sci.* **12**, 5286–5294 (2021).
234. Bennett, K., Kowalewski, M., Rouxel, J. R. & Mukamel, S. Monitoring molecular nonadiabatic dynamics with femtosecond X-ray diffraction. *Proc. Natl Acad. Sci. USA* **115**, 6538–6547 (2018).
235. Shakya, Y., Inhester, L., Arnold, C., Welsch, R. & Santra, R. Ultrafast time-resolved X-ray absorption spectroscopy of ionized urea and its dimer through ab initio nonadiabatic dynamics. *Struct. Dyn.* **8**, 034102 (2021).
236. List, N. H., Dempwolff, A. L., Dreuw, A., Norman, P. & Martínez, T. J. Probing competing relaxation pathways in malonaldehyde with transient X-ray absorption spectroscopy. *Chem. Sci.* **11**, 4180–4193 (2020).
237. Keefer, D., Schnappinger, T., de Vivie-Riedle, R. & Mukamel, S. Visualizing conical intersection passages via vibronic coherence maps generated by stimulated ultrafast X-ray Raman signals. *Proc. Natl Acad. Sci. USA* **117**, 24069–24075 (2020).
238. Nenov, A., Segatta, F., Bruner, A., Mukamel, S. & Garavelli, M. X-ray linear and non-linear spectroscopy of the ESCA molecule. *J. Chem. Phys.* **151**, 114110 (2019).
239. Kowalewski, M. Catching conical intersections in the act: monitoring transient electronic coherences by attosecond stimulated X-ray Raman signals. *Phys. Rev. Lett.* **115**, 193003 (2015).
240. Rouxel, J. R., Kowalewski, M., Bennett, K. & Mukamel, S. X-ray sum frequency diffraction for direct imaging of ultrafast electron dynamics. *Phys. Rev. Lett.* **120**, 243902 (2018).
241. Neville, S. P., Chergui, M., Stolow, A. & Schuurman, M. S. Ultrafast X-ray spectroscopy of conical intersections. *Phys. Rev. Lett.* **120**, 243001 (2018).
242. Keefer, D. et al. Imaging conical intersection dynamics during azobenzene photoisomerization by ultrafast X-ray diffraction. *Proc. Natl Acad. Sci. USA* **118**, e2022037118 (2021).
243. Amann, J. et al. Demonstration of self-seeding in a hard-X-ray free-electron laser. *Nat. Photon.* **6**, 693–698 (2012).
244. Cavaletto, S. M., Keefer, D. & Mukamel, S. High temporal and spectral resolution of stimulated X-ray Raman signals with stochastic free-electron-laser pulses. *Phys. Rev. X* **11**, 011029 (2021).
245. Biggs, J. D., Zhang, Y., Healion, D. & Mukamel, S. Watching energy transfer in metalloporphyrin heterodimers using stimulated X-ray Raman spectroscopy. *Proc. Natl Acad. Sci. USA* **110**, 15597–15601 (2013).
246. Kimberg, V. et al. Stimulated X-ray Raman scattering — a critical assessment of the building block of nonlinear X-ray spectroscopy. *Faraday Discuss.* **194**, 305–324 (2016).
247. Gschwendtner, E. & Muggli, P. Plasma wakefield accelerators. *Nat. Rev. Phys.* **1**, 246–248 (2019).
248. Wang, W. et al. Free-electron lasing at 27 nanometres based on a laser wakefield accelerator. *Nature* **595**, 516–520 (2021).
249. Galletti, M. et al. Stable operation of a free-electron laser driven by a plasma accelerator. *Phys. Rev. Lett.* **129**, 234801 (2022).
250. Labat, M. et al. Seeded free-electron laser driven by a compact laser plasma accelerator. *Nat. Photon.* **17**, 150–156 (2023).
251. Trebino, R. *Frequency-Resolved Optical Gating: The Measurement of Ultrashort Laser Pulses: The Measurement of Ultrashort Laser Pulses* (Springer Science & Business Media, 2000).
252. Peters, W. K. et al. All-optical single-shot complete electric field measurement of extreme ultraviolet free electron laser pulses. *Optica* **8**, 545–550 (2021).
253. Gauthier, D. et al. Spectrotemporal shaping of seeded free-electron laser pulses. *Phys. Rev. Lett.* **115**, 114801 (2015).
254. Prince, K. C. et al. Coherent control with a short-wavelength free-electron laser. *Nat. Photon.* **10**, 176–179 (2016).
255. Cavaletto, S. M. et al. Unveiling the spatial distribution of molecular coherences at conical intersections by covariance X-ray diffraction signals. *Proc. Natl Acad. Sci. USA* **118**, e2105046118 (2021).
256. Ratner, D., Cryan, J. P., Lane, T. J., Li, S. & Stupakov, G. Pump–probe ghost imaging with SASE FELs. *Phys. Rev. X* **9**, 011045 (2019).
257. Kayser, Y. et al. Core-level nonlinear spectroscopy triggered by stochastic X-ray pulses. *Nat. Commun.* **10**, 4761 (2019).
258. Driver, T. et al. Attosecond transient absorption spectroscopy: a ghost imaging approach to ultrafast absorption spectroscopy. *Phys. Chem. Chem. Phys.* **22**, 2704–2712 (2020).
259. Gorobtsov, O. Y. et al. Seeded X-ray free-electron laser generating radiation with laser statistical properties. *Nat. Commun.* **9**, 4498 (2018).
260. Li, K. et al. Ghost-imaging-enhanced noninvasive spectral characterization of stochastic X-ray free-electron-laser pulses. *Commun. Phys.* **5**, 1–8 (2022).
261. Kalz, K. F. et al. Future challenges in heterogeneous catalysis: understanding catalysts under dynamic reaction conditions. *ChemCatChem* **9**, 17–29 (2017).
262. Yang, Y. et al. Operando methods in electrocatalysis. *ACS Catal.* **11**, 1136–1178 (2021).
263. Singh, J., Lamberti, C. & van Bokhoven, J. A. Advanced X-ray absorption and emission spectroscopy: in situ catalytic studies. *Chem. Soc. Rev.* **39**, 4754–4766 (2010).
264. Beye, M. et al. Non-linear soft X-ray methods on solids with MUSIX — the multi-dimensional spectroscopy and inelastic X-ray scattering endstation. *J. Phys. Condens. Matter* **31**, 014003 (2019).
265. Chakraborti, P. et al. Higher-order X-ray — optical wave mixing. *SPring-8/SACLA*利用研究成果集 https://doi.org/10.18957/rr.10.4.409 (2022).
266. Alagna, L. et al. X-ray natural circular dichroism. *Phys. Rev. Lett.* **80**, 4799–4802 (1998).
267. Peacock, R. D. & Stewart, B. Natural circular dichroism in X-ray spectroscopy. *J. Phys. Chem. B* **105**, 351–360 (2001).
268. Turchini, S. et al. Core electron transitions as a probe for molecular chirality: natural circular dichroism at the carbon K-edge of methyloxirane. *J. Am. Chem. Soc.* **126**, 4532–4533 (2004).
269. Tanaka, M., Nakagawa, K., Agui, A., Fujii, K. & Yokoya, A. First observation of natural circular dichroism for biomolecules in soft X-ray region studied with a polarizing undulator. *Phys. Scr.* **2005**, 873 (2005).
270. Rouxel, J. R. et al. Hard X-ray helical dichroism of disordered molecular media. *Nat. Photon.* **16**, 570–574 (2022).
271. Mincigrucci, R. et al. Element- and enantiomer-selective visualization of molecular motion in real-time. *Nat. Commun.* **14**, 386 (2023).
272. Byers, J. D., Yee, H. I., Petralli-Mallow, T. & Hicks, J. M. Second-harmonic generation circular-dichroism spectroscopy from chiral monolayers. *Phys. Rev. B* **49**, 14643–14647 (1994).
273. Petralli-Mallow, T., Wong, T. M., Byers, J. D., Yee, H. I. & Hicks, J. M. Circular dichroism spectroscopy at interfaces: a surface second harmonic generation study. *J. Phys. Chem.* **97**, 1383–1388 (1993).
274. Kauranen, M., Verbiest, T., Maki, J. J. & Persoons, A. Second-harmonic generation from chiral surfaces. *J. Chem. Phys.* **101**, 8193–8199 (1994).
275. Verbiest, T., Kauranen, M., Van Rompaey, Y. & Persoons, A. Optical activity of anisotropic achiral surfaces. *Phys. Rev. Lett.* **77**, 1456–1459 (1996).

276. Verbiest, T., Kauranen, M. & Persoons, A. Second-order nonlinear optical properties of chiral thin films. *J. Mater. Chem.* **9**, 2005–2012 (1999).
277. Belkin, M. A., Han, S. H., Wei, X. & Shen, Y. R. Sum-frequency generation in chiral liquids near electronic resonance. *Phys. Rev. Lett.* **87**, 113001 (2001).
278. Belkin, M. A., Shen, Y. R. & Flytzanis, C. Coupled-oscillator model for nonlinear optical activity. *Chem. Phys. Lett.* **363**, 479–485 (2002).
279. Belkin, M. A. & Shen, Y. R. Non-linear optical spectroscopy as a novel probe for molecular chirality. *Int. Rev. Phys. Chem.* **24**, 257–299 (2005).
280. Fischer, P., Beckwitt, K., Wise, F. W. & Albrecht, A. C. The chiral specificity of sum-frequency generation in solutions. *Chem. Phys. Lett.* **352**, 463–468 (2002).
281. Lee, T., Rhee, H. & Cho, M. Femtosecond vibrational sum-frequency generation spectroscopy of chiral molecules in isotropic liquid. *J. Phys. Chem. Lett.* **9**, 6723–6730 (2018).
282. Song, Z., Zhang, T., Fang, Z. & Fang, C. Quantitative mappings between symmetry and topology in solids. *Nat. Commun.* **9**, 3530 (2018).
283. Gatti, G. et al. Radial spin texture of the Weyl fermions in chiral tellurium. *Phys. Rev. Lett.* **125**, 216402 (2020).
284. Cochran, T. A. et al. Visualizing higher-fold topology in chiral crystals. *Phys. Rev. Lett.* **130**, 066402 (2023).
285. Rouxel, J. R., Kowalewski, M. & Mukamel, S. Photoinduced molecular chirality probed by ultrafast resonant X-ray spectroscopy. *Struct. Dyn.* **4**, 044006 (2017).
286. Rouxel, J. R., Zhang, Y. & Mukamel, S. X-ray Raman optical activity of chiral molecules. *Chem. Sci.* **10**, 898–908 (2019).
287. Bencivenga, F. et al. Four-wave-mixing experiments with seeded free electron lasers. *Faraday Discuss.* **194**, 283–303 (2016).
288. Rouxel, J. R. & Mukamel, S. Molecular chirality and its monitoring by ultrafast X-ray pulses. *Chem. Rev.* **122**, 16802–16838 (2022).
289. Rouxel, J. R., Rajabi, A. & Mukamel, S. Chiral four-wave mixing signals with circularly polarized X-ray pulses. *J. Chem. Theory Comput.* **16**, 5784–5791 (2020).
290. Schenkl, S. et al. Insights into excited-state and isomerization dynamics of bacteriorhodopsin from ultrafast transient UV absorption. *Proc. Natl Acad. Sci. USA* **103**, 4101–4106 (2006).
291. Polli, D. et al. Conical intersection dynamics of the primary photoisomerization event in vision. *Nature* **467**, 440–443 (2010).
292. Schreier, W. J., Gilch, P. & Zinth, W. Early events of DNA photodamage. *Annu. Rev. Phys. Chem.* **66**, 497–519 (2015).
293. Ebadi, H. Tracking of azobenzene isomerization by X-ray emission spectroscopy. *J. Phys. Chem. A* **118**, 7832–7837 (2014).
294. Hua, W., Mukamel, S. & Luo, Y. Transient X-ray absorption spectral fingerprints of the S1 dark state in uracil. *J. Phys. Chem. Lett.* **10**, 7172–7178 (2019).
295. Nam, Y. et al. Time-resolved optical pump-resonant X-ray probe spectroscopy of 4-thiouracil: a simulation study. *J. Chem. Theory Comput.* **18**, 3075–3088 (2022).
296. Segatta, F. et al. Exploring the capabilities of optical pump X-ray probe NEXAFS spectroscopy to track photo-induced dynamics mediated by conical intersections. *Faraday Discuss.* **221**, 245–264 (2020).
297. Chang, K. F. et al. Revealing electronic state-switching at conical intersections in alkyl iodides by ultrafast XUV transient absorption spectroscopy. *Nat. Commun.* **11**, 4042 (2020).
298. Timmers, H. et al. Disentangling conical intersection and coherent molecular dynamics in methyl bromide with attosecond transient absorption spectroscopy. *Nat. Commun.* **10**, 3133 (2019).
299. Nam, Y. et al. Conical intersection passages of molecules probed by X-ray diffraction and stimulated Raman spectroscopy. *J. Phys. Chem. Lett.* **12**, 12300–12309 (2021).
300. Freixas, V. M., Keefer, D., Tretiak, S., Fernandez-Alberti, S. & Mukamel, S. Ultrafast coherent photoexcited dynamics in a trimeric dendrimer probed by X-ray stimulated-Raman signals. *Chem. Sci.* **13**, 6373–6384 (2022).
301. Polishchuk, S. et al. Nanoscale-resolved surface-to-bulk electron transport in $CsPbBr_3$ perovskite. *Nano Lett.* **22**, 1067–1074 (2022).
302. Consani, C., Bram, O., van Mourik, F., Cannizzo, A. & Chergui, M. Energy transfer and relaxation mechanisms in cytochrome c. *Chem. Phys.* **396**, 108–115 (2012).
303. Chenu, A. & Scholes, G. D. Coherence in energy transfer and photosynthesis. *Annu. Rev. Phys. Chem.* **66**, 69–96 (2015).
304. Bacellar, C. et al. Ultrafast energy transfer from photoexcited tryptophan to the haem in cytochrome c. *J. Phys. Chem. Lett.* **14**, 2425–2432 (2023).
305. Zeiger, H. J. et al. Theory for displacive excitation of coherent phonons. *Phys. Rev. B* **45**, 768–778 (1992).
306. Mukamel, S., Healion, D., Zhang, Y. & Biggs, J. D. Multidimensional attosecond resonant X-ray spectroscopy of molecules: lessons from the optical regime. *Annu. Rev. Phys. Chem.* **64**, 101–127 (2013).
307. Al-Haddad, A. et al. Observation of site-selective chemical bond changes via ultrafast chemical shifts. *Nat. Commun.* **13**, 7170 (2022).
308. El Nahhas, A. et al. X-ray absorption spectroscopy of ground and excited rhenium-carbonyl diimine-complexes: evidence for a two-center electron transfer. *J. Phys. Chem. A* **117**, 361–369 (2013).
309. Bencivenga, F. & Masciovecchio, C. FEL-based transient grating spectroscopy to investigate nanoscale dynamics. *Nucl. Instrum. Methods Phys. Res. Sect. Accel. Spectrometers Detect. Assoc. Equip.* **606**, 785–789 (2009).
310. Johnson, J. A. et al. Direct measurement of room-temperature nondiffusive thermal transport over micron distances in a silicon membrane. *Phys. Rev. Lett.* **110**, 025901 (2013).

Acknowledgements
S.M. gratefully acknowledges the support of the Chemical Sciences, Geosciences and Biosciences Division, Office of Basic Energy Sciences, Office of Science, U.S. Department of Energy through Award No. DE-FG02-04ER15571 and of the National Science Foundation (Grant No. CHE-2246379). M.C. thanks the Swiss NSF NCCR:MUST and the ERC Advanced Grant DYNAMOX for support. All authors are deeply grateful to their former students and postdocs and to their collaborators for making this work possible.

Author contributions
M.C. researched data for the article. All authors contributed substantially to discussion of the content. M.C. and S.M. wrote the article. All authors reviewed and/or edited the manuscript before submission.

Competing interests
The authors declare no competing interests.

Additional information
Peer review information *Nature Reviews Physics* thanks Nora Berrah and the other, anonymous, reviewer(s) for their contribution to the peer review of this work.

Publisher's note Springer Nature remains neutral with regard to jurisdictional claims in published maps and institutional affiliations.